

Systematic effects of the quenched approximation on the strong penguin contribution to ϵ'/ϵ

C. Aubin,¹ N. H. Christ,¹ C. Dawson,² J.W. Laiho,^{3,4,5} J. Noaki,^{2,6} S. Li,¹ and A. Soni³

¹*Physics Department, Columbia University, New York, NY 10027*

²*RIKEN-BNL Research Center, Brookhaven National Laboratory, Upton, NY 11973*

³*Physics Department, Brookhaven National Laboratory, Upton, NY 11973*

⁴*Physics Department, Princeton University, Princeton, NJ 08544*

⁵*Present address: Physics Department, Fermilab, Batavia, IL 60510*

⁶*Present address: School of Physics and Astronomy,
University of Southampton, Southampton, SO17 1BJ, England*

We discuss the implementation and properties of the quenched approximation in the calculation of the left-right, strong penguin contributions (*i.e.* Q_6) to ϵ'/ϵ . The coefficient of the new chiral logarithm, discovered by Golterman and Pallante, which appears at leading order in quenched chiral perturbation theory is evaluated using both the method proposed by those authors and by an improved approach which is free of power divergent corrections. The result implies a large quenching artifact in the contribution of Q_6 to ϵ'/ϵ . This failure of the quenched approximation affects only the strong penguin operators and so does not affect the Q_8 contribution to ϵ'/ϵ nor $\text{Re}A_0$, $\text{Re}A_2$ and thus, the $\Delta I = 1/2$ rule at tree level in chiral perturbation theory.

PACS numbers: 11.15.Ha, 11.30.Rd, 12.38.Aw, 12.38.-t 12.38.Gc

I. INTRODUCTION

There have been several recent applications of lattice QCD to the calculation of $\text{Re}(\epsilon'/\epsilon)$, the direct CP violating parameters in $K \rightarrow \pi\pi$ decays. These include the attempts using domain wall fermions by the CP-PACS [1] and RBC [2] collaborations. A notable feature of both of these calculations is that their central values differ drastically from experiment. The experiments at CERN [3, 4] and Fermilab [5, 6] have yielded an experimental world average of $\text{Re}(\epsilon'/\epsilon) = (1.8 \pm 0.4) \times 10^{-3}$ [7]. The RBC collaboration reported a value $-4.0(2.3) \times 10^{-4}$, and a similar negative central value was reported by CP-PACS. (See [8] for an earlier attempt using staggered fermions and [9] for ongoing work also using staggered fermions.) The stated errors in the RBC lattice calculations for ϵ'/ϵ were statistical only, with an estimate of the size of the systematic errors requiring much further study, of which this work is part.

A number of serious approximations were made in the lattice calculations which introduced uncontrolled systematic errors. One of these was the quenched approximation, in which the fermion determinant is ignored in the generation of the gauge configurations. This is a truncation of the full theory that dramatically reduces the computer resources required, but is uncontrolled. Where quenched lattice results have been compared to experiment, in simple quantities such as masses of flavored mesons and decay constants, the agreement is at or better than $\sim 15\%$. However, there is no apparent reason for this level of agreement to hold for all low-energy hadronic phenomena. Another approximation made in all existing lattice calculations of ϵ'/ϵ was the use of leading order chiral perturbation theory (ChPT) to relate unphysical $K \rightarrow \pi$ and $K \rightarrow 0$ amplitudes to the physical $K \rightarrow \pi\pi$ amplitudes, as first proposed by [10]. This is also likely to be a serious source of systematic error, although in this paper we focus on a particular ambiguity present in the quenched approximation.

Since the original lattice calculations of [1, 2], it was shown in [11, 12] that, at leading order in quenched chiral perturbation theory there is a term logarithmic in the pion mass which contributes to the matrix elements of the strong penguin operators. This term is absent in full QCD, and its contribution is proportional to an *a priori* unknown, new low energy constant (LEC). In terms of a representation of quenched QCD in which the fermion loops are cancelled by the addition of ghost fields to the lagrangian, this LEC can be associated with the presence of additional operators in the effective hamiltonian mediating the weak

decay of $K \rightarrow \pi\pi$ which contain both quark and ghost fields. The presence of additional operators naturally calls for a re-examination of the way in which the quenched approximation is implemented in such matrix element calculations; without further guidance, a single strong penguin operator in the full theory can be represented by any arbitrary linear combination of its direct transcription into the quenched theory (a four-quark operator) and these additional (two-quark, two-ghost) operators.

Since this ChPT result only became known after the original RBC analysis was completed [2], that work used the leading order ChPT relevant for full QCD. As such, it is useful to discuss how the presence of these new operators might effect this result. We emphasize that this particular quenching difficulty is present only for the strong penguin operators and so does not affect the Q_8 contribution to ϵ'/ϵ . This quenching ambiguity also does not significantly affect $\text{Re } A_0$ and $\text{Re } A_2$ and since $\text{Re } A_0$ receives only a negligibly small contribution from Q_6 [2], the RBC result for the $\Delta I = 1/2$ rule remains unchanged. A recent paper by Golterman and Pallante [13] shows how similar quenched penguin effects can arise in the $\Delta I = 1/2$ rule, and thus change the values of the underlying LEC's that one measures. However, the effects of Ref. [13] do not change the tree-level results of Bernard, et al [10], and as the original RBC analysis was performed at tree level, this does not affect the actual results for the $\Delta I = 1/2$ rule. An attempt to determine the systematic error due to quenching for this quantity may, however, be influenced by the results of Golterman and Pallante.

Since the quenched approximation is uncontrolled, a rigorous matching of operators between the quenched and full theories is not possible. However, we argue that the coefficients of these new operators can be determined by the same style of physical argument that is usually put forward to motivate the quenched approximation. This approach, which might be called “intermediate-energy matching” can be described as follows. Since quark loops play an important role in the renormalization group evolution of the weak amplitudes from the scale of the W , Z and top quark down to the kaon mass, the quenched approximation must be applied in a discriminating fashion, simulating the vacuum polarization of quark loops in the low-energy lattice QCD calculation with a weakened bare coupling while leaving the quark loops that appear in the perturbatively computed Wilson coefficients intact.

Such a separation between short- and long-distance vacuum polarization effects can be made quite precise in the context of the effective weak Hamiltonian and gives a prescription

for carrying out the quenched calculation which is close to that adopted by RBC and CP-PACS. One simply requires at the intermediate energy scale at which the perturbatively determined weak amplitudes are matched to the low-energy four-quark operators in H_W that the full- and quenched-QCD amplitudes agree. Since there are no ghost quarks in the full theory, this requires that the ghost quark matrix elements of H_W evaluated in the quenched theory also vanish. This gives a physically motivated definition of the quenched approximation for the energy scale at which this matching is performed. Of course, as the quenched and full theories do not have the same low energy limit, physical results will depend on this matching scale; for the quenched approximation to be useful, the difference in these results as the matching scale is varied over the range of energy scales important for the quantities we are calculating must be numerically small. The extent to which this condition is obeyed depends on the quantity calculated; later we argue that for the strong penguin operators, the quenched approximation is particularly bad.

Another possible guide we may take in transcribing the full QCD operators into the quenched theory is the extended chiral symmetry of this theory [11, 12]. Recall that when the ghost quarks are added to normal QCD, the original chiral symmetry, $SU_L(3) \times SU_R(3)$, which transforms only the normal quarks, expands into a larger, graded symmetry, $SU_L(3|3) \times SU_R(3|3)$ for the simplest case of three quarks u , d and s and three ghost quarks \tilde{u} , \tilde{d} and \tilde{s} .

As analyzed by Golterman and Pallante, the original operators appearing in H_W , transforming in specific representations of $SU_L(3) \times SU_R(3)$, take on new $SU_L(3|3) \times SU_R(3|3)$ quantum numbers. The new operators containing ghost quarks might then be chosen in a fashion to simplify the resulting representation of the extended $SU_L(3|3) \times SU_R(3|3)$ symmetry group while leaving the physical $SU_L(3) \times SU_R(3)$ behavior unchanged. However, since this extended $SU_L(3|3) \times SU_R(3|3)$ group is necessarily unphysical it is difficult to provide a convincing motivation for the mixture of ghost quarks chosen.

Thus, we believe that the quenched approximation can be applied to weak decays in a well-motivated way. One determines by “intermediate-energy matching”, the quenched effective Hamiltonian, H_W^{qh} , and then examines matrix elements of the resulting operators analytically for possible quenched chiral logarithms and numerically to make quenched predictions from the theory. The size of the quenched chiral logarithms should be viewed as a measure of the errors in the quenched approximation.

From this perspective, the study of the quenched chiral logarithm discovered by Golterman and Pallante and the new low energy constant, α_q^{NS} , which appears as its coefficient, is of central importance. In fact, these authors have proposed [12] a method for obtaining α_q^{NS} , directly from a lattice calculation. We show that there are difficulties using their method to obtain α_q^{NS} from lattice data using domain wall fermions, due to the presence of power divergences. However, motivated by their direct approach, we have found an improved method for obtaining α_q^{NS} that does not have these divergences. This is done by constructing an extension of the usual CPS symmetry arguments to the quenched case where both quark and “ghost” quark degrees of freedom are present.

Using our proposed method, we obtain a value of α_q^{NS} which is consistent with the value given by the large N_c approximation obtained by Golterman and Peris [14, 15]. The value obtained from the method proposed by Golterman and Pallante also yielded a value roughly in agreement with the others, but with a larger systematic error. This large value of α_q^{NS} has two important consequences: i) Large, non-analytic behavior in the quenched chiral limit which is absent in full QCD provides clear evidence of substantial systematic errors associated with the quenched approximation. ii) If these new quenched non-linearities are omitted from the functional forms used to extract the quenched LEC’s, even the analysis within the quenched approximation is likely to be incorrect.

In Section II we discuss the application of the quenched approximation to weak decay amplitudes and motivate the “intermediate-energy matching” approach described above. The chiral symmetry of partially quenched QCD and quenched chiral perturbation theory is reviewed in Sec. III. We follow the approach of Ref [11] and discuss the ambiguities of determining H_W^{qh} from this perspective. In Section IV we discuss Golterman and Pallante’s method [12] for obtaining the low energy constant, α_q^{NS} . We extend the usual CPS symmetry arguments for obtaining the form of the power divergent contributions to $\Delta I = 1/2$ matrix elements to the quenched case involving external ghost quark states. In Section V we use this extended symmetry, as well as numerical results, to show that the method of [12], when evaluated using domain wall fermions, suffers from ambiguities due to power divergent contributions.

In Section VI an alternative method for obtaining α_q^{NS} is proposed which does not have a divergent contribution and this method is used in Section VII to obtain a numerical value for this constant. Finally, the implications of this result are discussed in the conclusion,

Section VIII. Some useful formulae are given in Appendix A, our conventions are specified in detail in Appendix B, and a discussion of the one-loop ChPT calculation used in the numerical extrapolation to obtain α_q^{NS} is given in Appendix C.

II. QUENCHED APPROXIMATION IN WEAK DECAY AMPLITUDES

While the quenched approximation is widely used as a device to reduce the computational requirements of lattice QCD calculations, its implementation in the calculation of weak matrix elements deserves further discussion. The physical justification for this approximation is the hypothesis that the largest effect of the omitted quark loops is a modification of the running QCD coupling constant $\alpha_s(\mu)$ because of the omission of quark vacuum polarization. To the extent that this hypothesis holds true for a particular quantity of physical interest we can then compensate to a large extent for the effects of quenching on $\alpha_s(\mu)$ at a relevant physical scale μ by an appropriate weakening of the bare lattice coupling $\alpha_0 = g_0^2/4\pi$ where g_0 is the gauge coupling which appears directly in the lattice QCD Lagrangian. An important limitation of this justification is apparent from the scale dependence of $\alpha_s(\mu)$. This scale dependence will be different between the full and quenched theories so the equality $\alpha_s(\mu) = \alpha_s^{qh}(\mu)$ will be approximately true only over a limited range of scales μ .

Since a weak matrix element involves a large range of energy scales from the top quark mass down to Λ_{QCD} , a naive application of the quenched approximation to this entire energy range would be very inaccurate. However, because perturbation theory is used to describe most of this larger energy range, it is also not necessary to use the quenched approximation over the entire range. A clear view of this situation comes from considering some sample Feynman graphs representing the various ways that quark vacuum polarization loops can enter the gluonic penguin diagrams of interest.

The possible effects of quark vacuum polarization are illustrated in Figs. 1-4. In the first of these, Fig. 1, the quark loop is entirely contained in the short distance part of the graph. The vacuum polarization loop will be dominated by momenta on the order of the top mass and can be accurately treated in QCD perturbation theory. Contributions with loop momentum on the order of Λ_{QCD} , where perturbation theory would not be accurate, will be suppressed by a factor of $(\Lambda_{\text{QCD}}/m_{\text{top}})^2$

By contrast, the diagram shown in Fig. 2 contains a vacuum polarization loop that can

only contain low momentum. More precisely, once multiplicative charge and wave-function renormalization constants have been removed, any further contributions from large energies, for example $\mu \approx m_W$, will be suppressed by an additional factor of μ^2/m_W^2 . Thus this graph represents a potentially non-perturbative piece which requires lattice techniques to evaluate. In fact, the above quenching hypothesis is simply the statement that the most important effect of removing this quark loop is a change in the charge renormalization, a change that can be completely compensated by a corresponding change in the bare lattice coupling g_0^2 .

The diagram shown in Fig. 3 contains a vacuum polarization loop that can either enter a short- or long-distance part of the graph. These two possibilities are represented by the two dotted boxes shown in the figure. Because of the presence of the W propagator, the inner box is necessarily a “high-momentum” subgraph. However, important contributions can come from regions of momentum space in which the lines entering the vacuum polarization subgraph carry either small ($\approx \Lambda_{\text{QCD}}$) or large ($\approx m_W$) momentum. In the case that large momentum is involved, the outer dotted box surrounds what becomes a “high-momentum” subgraph with all internal lines carrying large momentum: a regime that can be evaluated perturbatively and one in which the quenched approximation should not be used. For the “low-momentum” case, the contribution will be non-perturbative and evaluation using lattice techniques, potentially using the quenched approximation, will be needed. Other momentum assignments for the lines in this outer box which include only a portion of the vacuum polarization subgraph will have more than four external quark lines, thereby having larger dimension and giving a contribution that is suppressed by a factor of $(\Lambda_{\text{QCD}}/m_W)^2$.

Finally, Fig. 4 shows a potentially more ambiguous case. Here, in addition to the possibility that the vacuum polarization loop is contained entirely within a high- or low-momentum subgraph, (the outer and inner dotted boxes respectively) it may also be partially in both, as indicated by the middle dotted box. It is this intermediate subgraph which requires special discussion. For the case that all the momentum in the subgraph contained in the outer dotted box is large, the vacuum polarization loop can be treated perturbatively without recourse to the quenched approximation. For the case that only the momentum contained in the inner loop is large and those in the remainder of the graph are small, non-perturbative techniques will be needed and the quenched approximation may be used. Thus, in this case the vacuum polarization loop may be removed, or equivalently, a cancelling loop of ghost quarks included.

However, for the case of the intermediate dotted box which cuts the quark loop, the vacuum polarization piece is one-half within the high momentum part (the contents of this intermediate dotted box) but one half is to be evaluated in the low-momentum part. Here it is less obvious whether this loop is to be included perturbatively (*i.e.* incorporated in a Wilson coefficient) or to be cancelled by an added ghost quark contribution. In the language of the effective weak Hamiltonian H_W , such a cancellation of this vacuum polarization graph would be achieved by including ghost operators in H_W .

This variety of roles played by QCD vacuum polarization graphs might suggest that a precise definition of the quenched approximation for the evaluation of weak matrix elements would require new and elaborate development. However, as the above examples suggest, the standard field theoretic formulation of the “effective” low energy theory nicely deals with all of these questions, providing an unambiguous separation of the decay amplitudes into short-distance perturbative parts in which no quenched approximation is made and long-distance parts that must be evaluated non-perturbatively, possibly within a quenched approximation. The potential ambiguity associated with the inclusion of ghost operators is resolved by the matching conditions that are imposed to define the quenched effective theory.

To be more concrete, consider the gluonic penguin portion of the effective low-energy weak Hamiltonian transforming in the $(8, 1)$ representation of $SU(3)_L \times SU(3)_R$ and written as a sum of four independent, dimension-six, four-quark operators:

$$H_W = c_3 Q_3 + c_4 Q_4 + c_5 Q_5 + c_6 Q_6 \quad (1)$$

where $\{c_i\}_{i=3-6}$ are the four Wilson coefficients and $\{Q_i\}_{i=3-6}$ the four, conventional gluonic penguin operators:

$$Q_3 = \sum_{q=u,d,s} \bar{s}_a \gamma^\mu (1 - \gamma^5) d_a \bar{q}_b \gamma^\mu (1 - \gamma^5) q_b \quad (2)$$

$$Q_4 = \sum_{q=u,d,s} \bar{s}_a \gamma^\mu (1 - \gamma^5) d_b \bar{q}_b \gamma^\mu (1 - \gamma^5) q_a \quad (3)$$

$$Q_5 = \sum_{q=u,d,s} \bar{s}_a \gamma^\mu (1 - \gamma^5) d_a \bar{q}_b \gamma^\mu (1 + \gamma^5) q_b \quad (4)$$

$$Q_6 = \sum_{q=u,d,s} \bar{s}_a \gamma^\mu (1 - \gamma^5) d_b \bar{q}_b \gamma^\mu (1 + \gamma^5) q_a. \quad (5)$$

A sum over the repeated color indices a and b is understood.

The above discussion of the contributions of the various vacuum polarization graphs to short- and long-distance physics mirrors closely the usual field-theoretic derivation of the

effective weak Hamiltonian in Eq. 1. The usual “factorization” of weak amplitudes into short- and long-distance parts realized by H_W provides exactly the needed separation of vacuum polarization effects into those that are correctly included using perturbation theory and those which are omitted in the quenched approximation—their effects being partially reproduced by a decrease in the bare coupling constant.

Let us briefly recall this correspondence. The matrix elements of the local effective weak Hamiltonian given in Eq. 1 will accurately reproduce those of the complete theory if those matrix elements involve momenta which are small compared to the scale of the W meson and top quark masses—the scale at which non-trivial structure for the weak interactions becomes visible.

Leading contributions in an expansion in $1/m_{top}^2$ and $1/m_W^2$ will come from regions of integration over internal momenta in which: a) All momenta in a particular subgraph are large. b) That subgraph contains any top quark and W boson internal lines, and c) That subgraph has itself the minimum number of external lines or, more precisely, represents the lowest possible mass dimension or largest possible degree of divergence. Under these circumstances, this subgraph can be treated as a structureless local composite operator made up of fields corresponding to the external lines of the subgraph. When evaluated, integration over this large-momentum region for the subgraph contributes to the coefficient c_i appearing in H_W .

In fact, the four coefficients $\{c_i\}_{i=3-6}$ can be simply defined as those required to make the complete and effective theories agree. Typically the Wilson operators $\{Q_i\}_{i=3-6}$ will be defined by normalization conditions specified at an energy scale μ making both the operators Q_i and coefficient functions c_i functions of this scale μ as well. Usually the scale μ is also the scale at which the c_i are determined by requiring specific Greens functions containing an H_W vertex to agree with those predicted by the complete theory.

The application of this effective field theory formalism to the definition of the quenched approximation for the evaluation of weak matrix elements is now quite straight-forward. The vacuum polarization graphs which contribute to the short-distance/high-momentum part of the above analysis will necessarily contribute to the Wilson coefficients, can be evaluated in perturbation theory and need not involve the quenched approximation. Vacuum polarization effects which involve low momentum will enter the matrix elements of the Wilson operators Q_i , will likely require non-perturbative techniques for evaluation and may be computed in

the quenched approximation.

Now the equality between matrix elements of the complete and the effective theories, imposed for four specific amplitudes at the scale μ will hold for a range of scales and a variety of matrix elements only to the extent that the quenched approximation is accurate and the matrix elements (e.g. $\langle \pi\pi|Q_i|K \rangle$) of the Q_i in the unquenched theory agree with those evaluated in the quenched theory with the bare coupling weakened to compensate for the omitted quark-anti-quark screening. Note, in this definition of the quenched approximation we are replacing the matrix elements of the operators Q_i , originally to be evaluated in full QCD, with matrix elements evaluated in a new theory: a theory in which ghost quarks have been introduced, following the procedures of Bernard and Golterman [16], to completely cancel the fermion determinant, and the gauge coupling at short distances has been decreased to compensate for this quark loop omission.

Finally, let us examine the potential ambiguity associated with vacuum polarization loops, such as those in Fig. 4, which contribute partially to the short-distance, perturbative Wilson coefficients and partially to the low-energy non-perturbative matrix elements. The “quenching” of the loop cut by the middle dotted box in Fig. 4 reduces to the question of whether we add to our four Wilson operators $\{Q_i\}_{i=3-6}$ of Eqs. 2-5 new operators which contain ghost quarks. In fact, in the quenched theory there are four additional operators which have the same symmetry under $SU(3)_L \times SU(3)_R$ as these original four operators:

$$Q_3^* = \sum_{\tilde{q}=\tilde{u},\tilde{d},\tilde{s}} \bar{s}_a \gamma^\mu (1 - \gamma^5) d_a \bar{\tilde{q}}_b \gamma^\mu (1 - \gamma^5) \tilde{q}_b \quad (6)$$

$$Q_4^* = \sum_{\tilde{q}=\tilde{u},\tilde{d},\tilde{s}} \bar{s}_a \gamma^\mu (1 - \gamma^5) d_b \bar{\tilde{q}}_a \gamma^\mu (1 - \gamma^5) \tilde{q}_b \quad (7)$$

$$Q_5^* = \sum_{\tilde{q}=\tilde{u},\tilde{d},\tilde{s}} \bar{s}_a \gamma^\mu (1 - \gamma^5) d_a \bar{\tilde{q}}_b \gamma^\mu (1 + \gamma^5) \tilde{q}_b \quad (8)$$

$$Q_6^* = \sum_{\tilde{q}=\tilde{u},\tilde{d},\tilde{s}} \bar{s}_a \gamma^\mu (1 - \gamma^5) d_b \bar{\tilde{q}}_b \gamma^\mu (1 + \gamma^5) \tilde{q}_a. \quad (9)$$

Including these operators in our quenched effective weak Hamiltonian will have the effect of introducing ghost quark loops which will (partially) cancel the problematic quark loop in Fig. 4.

However, given the discussion above, the most consistent approach to the quenched approximation is now clear. The effective, quenched weak Hamiltonian, H_w^{qh} should incorporate

all eight possible operators:

$$H_w^{qh} = \sum_{i=3}^6 \left\{ c_i Q_i + c_i^* Q_i^* \right\} \quad (10)$$

and the eight coefficients $\{c_i\}_{i=3-6}$ and $\{c_i^*\}_{i=3-6}$ should be chosen to make the matrix elements of H_w^{qh} and those of the complete theory agree as closely as possible. This “matching” condition should be imposed at a sufficiently large scale μ that the required, perturbative evaluation of the complete theory is justified. On the other hand, given the inconsistent μ dependence of quantities in the complete and quenched theories, the scale μ also should be chosen as close as possible to the low energy region in which the quenched matrix elements are to be evaluated to minimize these inconsistencies. The scale μ is thus an intermediate energy scale and this approach might be called intermediate energy matching.

How are these four new coefficients $\{c_i^*\}_{i=3,4,5,6}$ to be evaluated and what values are expected? These new coefficients can be fixed by imposing conditions on the new ghost-quark amplitudes that appear in the quenched theory. They can be evaluated by comparing the complete theory, evaluated perturbatively, with the quenched theory evaluated either perturbatively or non-perturbatively. Since the complete theory does not contain ghost quarks, we should require that specific two-quark/two-ghost-quark amplitudes should vanish in the quenched theory. This would appropriately be done at off-shell, non-exceptional momentum at the scale μ and be imposed on color mixed and unmixed and left- and right-handed flavor-singlet combinations of ghost quarks. If carried out in perturbation theory, the absence of ghost quark coupling in the complete theory simply requires that all the c_i^* vanish to leading order in α_s . The choice $c_i^* = 0|_{i=3,4,5,6}$ is precisely the quenched approximation used by RBC and CP-PACS in their quenched kaon decay calculations, [1, 2]. Because of the ghost quark couplings introduced by the self-contractions of Fig. 5, these c_i^* coefficients will be non-zero at order α_s . While it would not be especially difficult to calculate the $\{c_i^*\}_{i=3,4,5,6}$ to order α_s in perturbation theory or to evaluate them using the RI-MOM techniques employed for similar quantities by the RBC collaboration in Ref. [2], we expect that these effects will be quite small as were similar disconnected amplitudes that were evaluated in this earlier work.

The majority of numerical simulations and the discussion above has been focused on the quenched approximation, in which all vacuum polarization loops are dropped from the calculation. However, there is additional insight and a useful framework for analysis to be

obtained in the case of “partial quenching” when a portion of the fermion determinant is included in the calculation. An important example involves the use of the wrong number of sea quarks, working with two rather than three flavors as in [17]. In fact with a positive Dirac operator (such as with domain wall fermions) and the proper algorithm [18], one can simulate with a value of N_f varying continuously between 0 and 3. The discussion for the quenched case applies quite directly to this partially quenched case as well.

Again one attempts to approximate matrix elements computed in the full theory with those computed in the truncated theory without the full fermion determinant. The effects of the missing determinant are partially reproduced by adjusting the bare coupling to account for the missing polarization effects. Again the effective weak Hamiltonian to be used in a partially quenched theory should be chosen so that at an intermediate matching point, the full and the partially quenched theory agree. Clearly as $N_f \rightarrow 3$ this approximation will become increasingly accurate as the vacuum polarization effects of the two theories become identical.

Even in the case $N_f = 3$ one can consider a partially quenched theory in which the valence quark masses do not match with the sea quark masses in the fermion determinant. For this case, the above discussion of quenching is simplified, since the differences between fermion masses appearing in quark loops can be neglected at the matching scale μ . Thus, the effective weak Hamiltonian, written in terms of the valence quark fields, will be the same as that in the full theory. Often setting $m_{\text{val}} = m_{\text{sea}}$, which can always be done, is less interesting than using $m_{\text{val}} \neq m_{\text{sea}}$ together with analytic results to explore the chiral limit.

In this section we have proposed a definition of the quenched approximation which provides a natural and self-consistent application of the standard quenched approximation to the case of hadronic weak decays. Up to corrections which are likely small, the calculations of both the RBC and CP-PACS collaborations use this definition in their evaluations of the gluonic penguin contributions, [1, 2]. However, since such an approximation is necessarily *ad hoc* and not systematic it must be used with suspicion. If unphysical effects, such as the quenched chiral logarithms discovered by Golterman and Pallante and evaluated numerically below, turn out to be large (as we will see they do), then the quenched approximation to these gluonic penguin amplitudes should be abandoned.

III. REVIEW OF STRONG PENGUINS IN QUENCHED CHPT

Following Golterman and Pallante, we will now use chiral symmetry and chiral perturbation theory to study the effects of the quenched approximation on the gluonic penguin contributions to K meson decay. Chiral perturbation theory is an important tool which provides an approximation scheme in which two-pion decay amplitudes can be computed from vacuum and single-pion transition amplitudes. It can also provide an indication of the accuracy of the quenched approximation by identifying unphysical, quenched singularities which give rise to the infamous “quenched chiral logarithms”.

In order to exploit chiral symmetry in the quenched approximation, we must adopt a field-theoretic description of quenching. This can be done in two ways: the supersymmetric formulation [16] and the replica method [19]. As in the discussion above, we will adopt the original supersymmetric formulation and use the quenched chiral perturbation theory of Bernard and Golterman [16]. In this method, the valence quarks are quenched by introducing ghost quarks which have the same mass and quantum numbers as the valence quarks but opposite statistics. Therefore the ghost loops cancel the loops of the valence quarks, effectively setting the fermion determinant to a constant, which is precisely the quenched approximation. The chiral symmetry group of this action is $SU(n|n)_L \times SU(n|n)_R$, a graded symmetry group, where n is the number of valence quark flavors. We adopt the definitions and notation of Bernard and Golterman [16] needed for this supersymmetric approach (see also Ref. [20]).

As in Ref. [21], one can also consider the partially quenched case, in which N sea quarks are introduced into the theory. In the notation of [21], one has n quarks, N of which are sea quarks, so that there are $n - N$ valence and, in addition, $n - N$ ghost quarks. The valence quarks have arbitrary mass, while the sea quarks are chosen to be degenerate. In this case, the graded chiral symmetry group of the action is $SU(n|n - N)_L \times SU(n|n - N)_R$.

A. Notation and graded groups

We will need to identify representations of the graded symmetry $SU(n|n - N)$ group and will adopt the following notation. Since the fundamental representation of $SU(N)$ and its complex conjugate are usually denoted, N and \overline{N} , we will adopt a similar description

of those representations of $SU(n|n-N)$: $(n|n-N)$ and $\overline{(n|n-N)}$. Thus, for example, a quark bilinear of the form $\overline{\mathcal{Q}}(1 + \gamma^5)\mathcal{Q}'$, will belong to a representation easily identified as $\overline{(n|n-N)}_L, (n|n-N)_R$. Here we use \mathcal{Q} to represent a column vector whose first n components are the anti-commuting quark fields q and whose final $n-N$ components are the ghost quark fields \tilde{q} . Likewise the quark bilinear $\overline{\mathcal{Q}}\gamma^\mu(1 + \gamma^5)\mathcal{Q}'$ will belong to the product representation $(1(n|n-N)_L, \overline{(n|n-N)}_R) \times (n|n-N)_R$ where we use the notation $1(n|n-N)$ to identify the trivial representation of the group $SU(n|n-N)$. This representation is easily constructed as the $(2n-N) \times (2n-N)$ identity matrix $I_{a,b}^{(n|n-N)}$, where the indices a and b transform as elements of the $(n|n-N)$ and $\overline{(n|n-N)}$ representations of $SU(n|n-N)$ respectively. This matrix has supertrace (defined below in Eq. 18 and Ref. [20]) $\text{str}(I^{(n|n-N)}) = N$.

We will be interested in two irreducible representations which appear in the product $\overline{(n|n-N)} \times (n|n-N)$ above. The first is the trivial representation $1(n|n-N)$ already discussed. The second is the adjoint representation which we denote as $\text{adj}(n|n-N)$. This is the representation formed from the $(2n-N)^2 - 1$ generators $T_{a,b}^i$ of the group $SU(n|n-N)$. Here i identifies the element of $\text{adj}(n|n-N)$ while the indices a and b transform as elements of the $(n|n-N)$ and $\overline{(n|n-N)}$ representations of $SU(n|n-N)$ respectively. Since the matrices U defining $SU(n|n-N)$ have unit superdeterminant, $\text{sdet}(U)=1$, the generators T^i each have vanishing supertrace: $\text{str}(T^i) = 0$. For the case $N \neq 0$, the trivial and adjoint representations are entirely distinct. Operators belonging to $1(n|n-N)$ cannot mix with those in $\text{adj}(n|n-N)$; the latter have a vanishing supertrace while the former do not.

However, for the quenched case where there are no sea quarks, $N = 0$, their supertraces both vanish and an operator in the $\text{adj}(n|n)$ representation can mix with a $1(n|n)$ operator. In fact, in the quenched, $N = 0$ case, the multiplication of the $2n$ fields q and \tilde{q} by a common phase factor has superdeterminant 1 making the unit matrix $I_{a,b}^{(n|n)}$ a valid generator of $SU(n|n)$ which is no longer simple in this $N = 0$ case. Thus, for the case $N = 0$ the adjoint representation, $\text{adj}(n|n)$, continues to have dimension $(2n)^2 - 1$ but now includes the identity matrix $I^{(n|n)}$. Of course there are still anti-hermitian matrices with non-vanishing supertrace. To include these we must extend the adjoint representation to a larger $(2n)^2$ -dimensional representation, denoted here $\overline{\text{adj}}(n|n)$ which includes the vectors in $\text{adj}(n|n)$.

Therefore, the product representation $\overline{(n|n)} \times (n|n)$ must be decomposed in an unfamiliar way. In contrast with the $N \neq 0$ case, this representation is not reducible and cannot be

written as a direct sum of $\text{adj}(n|n - N)$ and $1(n|n - N)$. The equation

$$\overline{(n|n - N)} \times (n|n - N) = \text{adj}(n|n - N) + 1(n|n - N) \quad (11)$$

does not apply for the case $N = 0$. Instead this product forms the irreducible representation $\overline{\text{adj}}(n|n)$. Contained within the $(2n)^2$ -dimensional supervector space on which this representation acts is an invariant supervector subspace of dimension $(2n)^2 - 1$ which forms the representation $\text{adj}(n|n)$. Finally this supervector subspace of dimension $(2n)^2 - 1$ itself contains a one-dimensional subspace which is again invariant under the original $\overline{\text{adj}}(n|n)$ representation matrices, transforming as the trivial $1(n|n)$ representation:

$$\overline{(n|n)} \times (n|n) = \overline{\text{adj}}(n|n) \supset \text{adj}(n|n) \supset 1(n|n) \quad (12)$$

The characteristics of this quenched, $N = 0$ case will be discussed further below.

B. Quenched chiral symmetry of Q_6

Let us now examine the effect that the quenched approximation has on the chiral symmetry properties of the gluonic penguin operator Q_6 , the four-quark operator which is expected, along with Q_8 , to make the largest contribution to ϵ'/ϵ . Our discussion builds on that of Golterman and Pallante[11, 12]. Recall that in the effective weak Hamiltonian for the full theory the Q_6 operator is given by Eq. 5, repeated here for convenience:

$$Q_6 = \bar{s}_a \gamma_\mu (1 - \gamma^5) d_b \sum_q \bar{q}_b \gamma^\mu (1 + \gamma^5) q_a. \quad (13)$$

The right-hand factor in this operator is a sum over light flavors, $q = u, d, s$, so in the full theory this factor is a flavor singlet under the symmetry group $SU(3)_R$. As discussed in the previous section, in the (partially) quenched theory, vacuum polarization effects permit this operator to mix with a new operator which contains sea and ghost quarks and belongs to the singlet representation of $SU(n|n - N)_R$:

$$Q_6^S = \bar{s}_a \gamma_\mu (1 - \gamma^5) d_b \sum_{\mathcal{Q}} \bar{\mathcal{Q}}_b \gamma^\mu (1 + \gamma^5) \mathcal{Q}_a. \quad (14)$$

where the sum over \mathcal{Q} contains all valence, sea and ghost quarks. An appropriate multiple of this operator can be subtracted from the original Q_6 operator, to create a new operator which transforms in the adjoint representation of $SU(n|n - N)_R$:

$$Q_6^{\text{adj}} = Q_6 - \frac{3}{N} Q_6^S. \quad (15)$$

Here the factor of $3/N$ is easily chosen so that the adjoint operator Q_6^{adj} has a vanishing supertrace. Following Golterman and Pallante, we re-order Eq. 15 to express the original operator Q_6 in terms of Q_6^{adj} and Q_6^S :

$$Q_6 = Q_6^{adj} + \frac{3}{N}Q_6^S. \quad (16)$$

This is a useful equation because the adjoint representation, to which Q_6^{adj} belongs, also includes the usual electro-weak penguin operator Q_8 so the matrix elements of these two operators are connected by a simple supersymmetry transformation. In addition, the NLO chiral perturbation theory for the relevant matrix elements of Q_6^S has been worked out.

As is evident from these equations, this useful decomposition does not work in the truly quenched case where $N = 0$. In this case, Golterman and Pallante propose defining a non-singlet operator Q_6^{NS} through the equation:

$$Q_6 = Q_6^{QNS} + \frac{1}{2}Q_6^{QS}. \quad (17)$$

where we have added the extra Q to the superscript of the general operator Q_6^S defined in Eq. 14 to emphasize that it is being defined for the quenched ($N = 0$) case. At first glance, Eq. 17 might offer the possibility of distinguishing two distinct contributions to Q_6 : due to Q_6^{QNS} and Q_6^{QS} , based upon their different chiral transformation properties under the graded symmetry. In turn this separation could – perhaps – be used to motivate an alternative definition of the quenched approximation, in which the non-singlet piece is dropped. Unfortunately, the decomposition in Eq. 17 is entirely arbitrary. The “non-singlet” operator, Q_6^{QNS} is not protected by the graded symmetry from mixing with the singlet operator. It is therefore ambiguous to separate out the “singlet piece” of Q_6 ; any amount of Q_6^{QS} could be added to the definition of Q_6^{QNS} , allowing the coefficient of $1/2$ in Eq. 17 to be replaced by any arbitrary number. In the representation theory language of the previous section, Q_6^{QS} is actually contained within the representation to which Q_6^{QNS} belongs: $1(n|n) \subset \overline{\text{adj}}(n|n)$. Thus, we cannot use Eq. 17 to identify a possibly preferred “singlet” part of the original Q_6 operator. It should be noted that Q_6^{QS} is protected by the graded symmetry from mixing with non-singlet operators; our conclusion due to the preceding arguments is simply that, since it is impossible to unambiguously define the singlet piece of Q_6 , any such approach is difficult to motivate physically.

For concreteness, we have focused on the specific operator Q_6 . However, the transformation properties of the other three gluonic operators are quite similar. The operator Q_5

transforms in an identical fashion as does Q_6 and these will of course mix when the energy scale at which they are defined is changed. The operators Q_3 and Q_4 are somewhat different since they transform only under $SU(n|n - N)_L$. While this increases the number of representations that can appear, the absence of right-handed indices makes their quenched chiral perturbation theory less singular.

We will now exploit these quenched chiral symmetry properties to study the matrix elements of these operators in the chiral limit.

C. Review of quenched ChPT

We now focus on the case of central interest in this work: quenched QCD, as above concentrating on the operator Q_6 . Since there are separate ChPT predictions for the matrix elements of the operators, Q_6 and Q_6^{QS} we will analyze them both in this paper. To leading order in QChPT these operators can be represented by

$$Q_6^{QS} = \alpha_{q1}^{QS} \text{str}[\lambda_6 \partial_\mu \Sigma \partial^\mu \Sigma^\dagger] + 2 \alpha_{q2}^{QS} B_0 \text{str}[\lambda_6 (M \Sigma^\dagger + \Sigma M^\dagger)] + \text{h.c.}, \quad (18)$$

$$Q_6 = \frac{1}{2} \{ \alpha_{q1}^{(8,1)} \text{str}[\lambda_6 \partial_\mu \Sigma \partial^\mu \Sigma^\dagger] + 2 \alpha_{q2}^{(8,1)} B_0 \text{str}[\lambda_6 (M \Sigma^\dagger + \Sigma M^\dagger)] + \text{h.c.} \} \\ + \alpha_q^{NS} \text{str}[\lambda_6 \Sigma \bar{A} \Sigma^\dagger] + \text{h.c.} \quad (19)$$

where $(\lambda_6)_{ij} = \delta_{i3} \delta_{j2}$ while

$$M = (m_u, m_d, m_s, m_u, m_d, m_s)_{\text{diag}}, \quad (20)$$

$$\bar{A} = (1, 1, 1, -1, -1, -1)_{\text{diag}}, \quad (21)$$

$$B_0 = \frac{m_{\pi^+}^2}{m_u + m_d} = \frac{m_{K^+}^2}{m_u + m_s} = \frac{m_{K^0}^2}{m_d + m_s}. \quad (22)$$

The matrix \bar{A} is an element of the extended adjoint representation $\overline{\text{adj}}(n|n)$ and appears here because the corresponding operator in the underlying quenched theory, defined in Eq. 17, transforms in the same fashion. The meson field Σ is defined by

$$\Sigma = \exp \left[\frac{2i\Phi}{f} \right] \quad (23)$$

with

$$\Phi \equiv \begin{pmatrix} \phi & \chi^\dagger \\ \chi & \tilde{\phi} \end{pmatrix}. \quad (24)$$

The quantity f is the pseudoscalar decay constant in the chiral limit (In the normalization used the physical value of the pion decay constant is $f_\pi \simeq 130$ MeV) while the 3×3 matrices ϕ , $\tilde{\phi}$ and χ^\dagger are constructed from Goldstone fields which create and destroy particles made from valence quarks and anti-quarks (bosons), ghost-anti-ghost quarks (bosons) and quarks and anti-ghost quarks (fermions) respectively.

We note that the ChPT representation for the operator Q_6 given in Eq. 18 differs from the implications of the original formula of Golterman and Pallante, Eq. 3.5 of Ref. [11]. In particular, the quenched non-singlet operator Q_6^{QNS} will be represented in chiral perturbation theory by both singlet and non-singlet operators. As a result, the low energy constants $\alpha_{q_1}^{(8,1)}$ and $\alpha_{q_2}^{(8,1)}$ which multiply the two quenched singlet operators which appear in Q_6 need not agree with the coefficients $\alpha_{q_1}^{QS}$ and $\alpha_{q_2}^{QS}$ which appear in the singlet operator Q_6^{QS} .

In Eqs. 18 and 19 and those below, we combine the $2n \times 2n$ matrix Σ together with the similar matrices \bar{A} and M , which appear in the quark-level theory, to form the most general set of operators that are invariant under the complete graded symmetry $S(n|n)_L \times SU(n|n)_R$ of the quenched theory, to a given order in the Goldstone particle masses and momenta. As matrices transforming in the product representation $(n|n) \times \overline{(n|n)}$ they can be written as:

$$U = \begin{pmatrix} A & B \\ C & D \end{pmatrix}, \quad (25)$$

where the sub-matrices have the same dimension as the sub-matrices of Φ , above. The invariance under the graded symmetry of the quenched theory requires the presence of supertraces in the operators of Eqs. 18 and 19 defined by

$$\text{str}(U) = \text{tr}(A) - \text{tr}(D). \quad (26)$$

To tree-level in ChPT, a pseudoscalar meson mass is given by

$$m_{ij}^2 = B_0(m_i + m_j), \quad (27)$$

where m_i and m_j are the masses of the two quarks that form the meson. We define m_{33} to be the tree-level meson mass of two valence strange quarks, as in [21]

$$m_{33}^2 = 2m_K^2 - m_\pi^2. \quad (28)$$

The new non-singlet operator of Eq. 19 is nominally of $O(p^0)$ in ChPT, but its tree-level contributions to physical matrix elements vanish because \bar{A} is proportional to the unit matrix

in the valence sector [12]. At $O(p^2)$ this is not true and the one-loop insertions of Q_6^{QNS} make a contribution of the same order as the tree-level insertions of Q_6^{QS} . Of course, there are additional non-singlet operators that can be constructed from the matrix \bar{A} which enter at $O(p^2)$ whose presence is needed to compensate for the scale dependence of the one-loop insertions of Q_6^{QNS} . This introduces three more LEC's into the amplitudes we must consider in this paper. The effective Lagrangian to this order is [12]:

$$\mathcal{L}_{NS}^{(NLO)} = \sum_i c_i^{NS} \mathcal{O}_i^{NS}, \quad (29)$$

with

$$\begin{aligned} \mathcal{O}_1^{NS} &= \text{str}[\lambda_6 L_\mu \Sigma^\dagger \bar{A} \Sigma L^\mu], \\ \mathcal{O}_3^{NS} &= \text{str}[\lambda_6 \{\Sigma^\dagger \bar{A} \Sigma, L^2\}], \\ \mathcal{O}_4^{NS} &= \text{str}[\lambda_6 \{\Sigma^\dagger \bar{A} \Sigma, S\}], \end{aligned} \quad (30)$$

and $S = 2B_0(M^\dagger \Sigma + \Sigma^\dagger M)$, $L_\mu = i\Sigma^\dagger \partial_\mu \Sigma$. In the following we work with operators renormalized in the \overline{MS} scheme, absorbing the divergence into the coefficients of the effective Lagrangian, which have the form

$$c_i^{NS} = c_i^{r,NS} + \frac{1}{16\pi^2 f^2} \left[\frac{1}{d-4} + \frac{1}{2}(\gamma_E - \ln 4\pi) \right] 2\alpha_q^{NS} \eta_i. \quad (31)$$

The finite coefficients, $c_i^{r,NS}$, are the renormalized low energy constants of the theory, while the factors η_i are chosen to cancel the divergences of the one-loop insertions of the tree-level operator. In the quenched theory we find $\eta_1 = 0$, $\eta_3 = 3$ and $\eta_4 = -3$. The scale dependence of the LEC's is given to one-loop order by

$$c_i^{r,NS}(\mu_2) = c_i^{r,NS}(\mu_1) + \frac{2\alpha_q^{NS} \eta_i}{(4\pi f)^2} \ln \frac{\mu_1}{\mu_2}, \quad (32)$$

where μ_1 and μ_2 are two different values of the chiral scale. The result for physical amplitudes should be independent of the scale and Eq. 32 is obtained by requiring that all one-loop amplitudes for the Q_6 operator be scale independent when the $O(p^2)$ NLO LEC's are included in the calculation.

The relations between our conventions for the LEC's and those of Golterman and Pallante [11, 12] are given below. The constant α_q^{NS} has been chosen to have a normalization that

agrees with that of $\alpha_q^{(8,8)}$ in Ref. [2]:

$$\alpha_{q,GP}^{NS} = \frac{2}{f^2} \alpha_q^{NS}. \quad (33)$$

In addition, we are working with the notation of Ref. [22] for the NLO LEC's. Although that work dealt with the electro-weak penguins, both transform in the $(\text{adj}(n|n-N)_L, \text{adj}(n|n-N)_R)$ representation of the partially quenched graded symmetry in the case $N \neq 0$ and we therefore keep that notation. The relationship between the two is

$$\begin{aligned} \beta_{q1}^{NS} &= (4\pi)^2 2c_3^{NS}, \\ \beta_{q2}^{NS} &= (4\pi)^2 2c_1^{NS}, \\ \beta_{q3}^{NS} &= (4\pi)^2 2c_4^{NS}. \end{aligned} \quad (34)$$

D. Q_6 amplitudes in quenched ChPT

We now review the ingredients necessary to obtain the contribution of both the operators Q_6^{QS} and Q_6 to the $K \rightarrow \pi\pi$ amplitude to leading order, $O(p^2)$, in quenched ChPT. The chiral behavior of Q_6^{QS} is the same as that of Q_6 in the full theory:

$$\langle \pi^+ \pi^- | Q_6^{QS} | K^0 \rangle = \frac{4i\alpha_{q1}^{QS}}{f^3} (m_K^2 - m_\pi^2), \quad (35)$$

where, as in the full QCD case, the needed LEC α_{q1}^{QS} can be extracted from the $K \rightarrow 0$ and $K \rightarrow \pi$ matrix elements:

$$\langle 0 | Q_6^{QS} | K^0 \rangle = \frac{4i\alpha_{q2}^{QS}}{f} (m_K^2 - m_\pi^2), \quad (36)$$

$$\langle \pi^+ | Q_6^{QS} | K^+ \rangle = \frac{4}{f^2} \alpha_{q1}^{QS} m_K m_\pi - \frac{4}{f^2} \alpha_{q2}^{QS} m_K^2. \quad (37)$$

The $K \rightarrow \pi\pi$ matrix element of Q_6 includes the one-loop contributions of α_q^{NS} and the

$O(p^2)$ LEC's, c_i^{NS} . In this case, $K \rightarrow \pi\pi$ is given by [12]:

$$\begin{aligned}
\langle \pi^+ \pi^- | Q_6 | K^0 \rangle &= \frac{4i}{f^3} \left(\frac{1}{2} \alpha_{q1}^{(8,1)} - c_1^{NS} - 2c_3^{NS} \right) (m_K^2 - m_\pi^2) \\
&+ \frac{2i}{16\pi^2 f^5} \alpha_q^{NS} \left[12(m_K^2 - m_\pi^2) \left(\ln \frac{m_\pi^2}{\mu^2} - 1 \right) \right. \\
&+ \left(\frac{m_K^6}{m_\pi^4} - 2 \frac{m_K^4}{m_\pi^2} + 2m_K^2 \right) \ln \frac{m_K^2}{m_\pi^2} \\
&+ \left(\frac{m_K^6}{m_\pi^4} - 6 \frac{m_K^4}{m_\pi^2} + 10m_K^2 - 4m_\pi^2 \right) \ln \frac{m_{33}^2}{m_\pi^2} \\
&+ 2m_K^2 \left(F(m_\pi^2, m_\pi^2, -m_K^2) - 2i\pi\theta(m_K^2 - 4m_\pi^2) \right. \\
&\times \sqrt{1 - \frac{4m_\pi^2}{m_K^2} + \frac{\pi}{3}\sqrt{3}} \left. + \left(\frac{m_K^4}{m_\pi^2} - 2m_K^2 \right) \right. \\
&\times \left. \left(2F(m_\pi^2, m_K^2, -m_\pi^2) + F(m_K^2, m_{33}^2, -m_\pi^2) \right) \right. \\
&\left. + 6m_K^2 \left(1 - \frac{m_K^2}{m_\pi^2} \right) \right], \tag{38}
\end{aligned}$$

where the function F is given in Appendix A. Note the scale dependence in the logarithmic term proportional to α_q^{NS} . This scale dependence cancels that of c_3^{NS} , as can be seen from Eq. 32. The Q_6 amplitudes for $K \rightarrow 0$ and $K \rightarrow \pi$ are [12]:

$$\begin{aligned}
\langle 0 | Q_6 | K^0 \rangle &= \frac{4i}{f} \left(\frac{1}{2} \alpha_{q2}^{(8,1)} + 2c_4^{NS} \right) (m_K^2 - m_\pi^2) \\
&+ \frac{8i}{f^3} \alpha_q^{NS} \frac{1}{16\pi^2} \left[m_K^2 \ln \frac{m_K^2}{\mu^2} - 2m_\pi^2 \ln \frac{m_\pi^2}{\mu^2} + m_{33}^2 \ln \frac{m_{33}^2}{\mu^2} \right. \\
&\left. - 3(m_K^2 - m_\pi^2) \right], \tag{39}
\end{aligned}$$

$$\langle \pi^+ | Q_6 | K^+ \rangle = \frac{4m_M^2}{f^2} \left(\frac{1}{2} \alpha_{q1}^{(8,1)} - \frac{1}{2} \alpha_{q2}^{(8,1)} - c_1^{NS} - 2c_3^{NS} - 2c_4^{NS} \right), \tag{40}$$

where in the expression for $K \rightarrow \pi$ we have set the quark masses to be degenerate ($m_K^2 = m_\pi^2 = m_M^2$), as in the numerical simulation [2]. Note, as discussed above, the singlet LEC's $\alpha_{q1}^{(8,1)}$ and $\alpha_{q2}^{(8,1)}$ entering the equations for Q_6 (Eqs. 38, 39 and 40) need not be the same as the corresponding LEC's, α_{q1}^{QS} and α_{q2}^{QS} appearing in the corresponding expressions for Q_6^{QS} (Eqs. 35, 36 and 37).

Notice that the same linear combinations of LEC's appear in the above three equations, $\alpha_{q1}^{(8,1)}/2 - c_1^{NS} - 2c_3^{NS}$ and $\alpha_{q2}^{(8,1)}/2 + 2c_4^{NS}$. If the value of α_q^{NS} is small, then the procedure for obtaining $K \rightarrow \pi\pi$ in which one neglects α_q^{NS} reduces to that of the full theory. In this

case, the previously mentioned combinations of LEC's replace $\alpha_1^{(8,1)}$ and $\alpha_2^{(8,1)}$, respectively. The strategy that was employed in Refs. [1] and [2] implicitly made this approximation.

It has recently been suggested, however, that the value of α_q^{NS} is large compared to the other LEC's in the amplitudes and cannot be neglected [14]. A large N_c expansion was used to obtain the result (in our conventions),

$$\alpha_q^{NS} = -\frac{1}{4}f^4 B_0^2. \quad (41)$$

When quenched lattice values for these constants are substituted into this equation, one finds that the resulting value of α_q^{NS} is so large that it cannot be ignored. The non-linearities implied by the presence of α_q^{NS} in Eq. 39 need to be included when this expression is used to extract the LEC's from the $K \rightarrow 0$ lattice data and the explicit form of the α_q^{NS} -dependent term in Eq. 38 needs to be taken into account in a quenched prediction for $K \rightarrow \pi\pi$. Of course, with such large quenching artifacts, such a quenched prediction will be of limited value.

It is therefore crucial to have a means for determining α_q^{NS} directly from a lattice calculation. Golterman and Pallante have provided a method for doing just that. However, we have found that their method suffers from ambiguities which are power divergent in the lattice spacing when employed in the case of domain wall fermions, making accurate extraction of α_q^{NS} from the lattice data rather difficult. In particular, with a finite L_s (the separation between the two physical, four-dimensional walls in the fifth dimension), this power divergent contribution, although suppressed by a factor of order of the residual chiral symmetry breaking, $O(m_{\text{res}})$, could be large. We discuss this difficulty in the following sections and present an alternative method for obtaining α_q^{NS} which avoids this problem.

IV. LATTICE DETERMINATION OF α_q^{NS} FROM $\tilde{K} \rightarrow 0$

In this section we review the method proposed by Golterman and Pallante to obtain α_q^{NS} on the lattice [12], together with the (CPS) symmetry arguments needed to understand the form of the power divergences in the matrix elements of four-quark operators. As will be explained in the following, Golterman and Pallante introduced a new operator, \tilde{Q}_6^{QNS} , and extracted α_q^{NS} from matrix elements of this operator which included ghost particles in the external states. By extending the standard CPS symmetry arguments to include quark-ghost

transformations, we show that this method suffers from contamination from terms which are power divergent in the lattice spacing. Nevertheless, we present numerical results from this approach. While these results are in rough agreement with the large N_c estimates [14], due to the ambiguities associated with the power divergence the results must be considered inconclusive; in Section VI we suggest an alternative approach which does not suffer from this problem.

A. Review of Golterman and Pallante's method

In Eq. 39 it is difficult to numerically disentangle the logarithmic α_q^{NS} term from the linear term and possible higher order effects. It was for this reason that a new matrix element was suggested in Ref. [12] to which α_q^{NS} contributes at $O(p^0)$, so that it may be obtained more readily in the chiral limit. This can be done if one considers a matrix element where the ghost quarks can appear on external lines. In order to obtain such a matrix element, one must perform an $SU(3|3)_L$ flavor rotation of the operator Q_6^{QNS} into

$$\begin{aligned}\tilde{Q}_6^{QNS} &= -\frac{1}{2}\bar{s}\gamma^\mu(1-\gamma^5)\tilde{d}\left(\sum_q\bar{q}\gamma^\mu(1+\gamma^5)q-\sum_{\tilde{q}}\bar{\tilde{q}}\gamma^\mu(1+\gamma^5)\tilde{q}\right) \\ &= -\frac{1}{2}\bar{\mathcal{Q}}\tilde{\lambda}_6\gamma^\mu(1-\gamma^5)\mathcal{Q}\bar{\mathcal{Q}}\bar{A}\gamma^\mu(1+\gamma^5)\mathcal{Q},\end{aligned}\tag{42}$$

where now the \tilde{d} is a ghost quark field. The matrix $\tilde{\lambda}_6$ is given by $(\tilde{\lambda}_6)_{ij} = \delta_{i3}\delta_{j5}$, a quenched chiral transform of the matrix λ_6 defined earlier. To leading order in ChPT, this operator is

$$\tilde{Q}_6^{QNS} = \alpha_q^{NS}\text{str}[\tilde{\lambda}_6\Sigma\bar{A}\Sigma^\dagger] + \text{h.c.}\tag{43}$$

Note that some care must be taken in order to maintain consistency in the sign conventions between the chiral and quark level operators. Our conventions are presented in detail in Appendix B. Since the above operator is in the same irreducible representation as Q_6^{QNS} , it is parameterized by the same low energy constants. Considering the matrix element $\tilde{K} \rightarrow 0$, we have, to leading order

$$\langle 0|\tilde{Q}_6^{QNS}|\tilde{K}^0\rangle = \frac{4i}{f}\alpha_q^{NS}.\tag{44}$$

Although this method isolates α_q^{NS} at leading order, the NLO contribution has a power divergent coefficient, making the numerical extraction problematic. We discuss the way in which the mixing of four-quark operators with power divergent lower dimensional operators can be constrained by the symmetries of the theory in the following subsection.

B. Power divergences and CPS symmetry

In general, the $\Delta I = 1/2$ matrix elements of four-quark operators have a power divergent part, due to mixing with lower dimensional operators. This power divergence will involve the quark bilinears, $\bar{s}d$ and $\bar{s}\gamma_5 d$, times a momentum independent coefficient [2]. One can define the following quark bilinear operator [10],

$$\Theta^{(3,\bar{3})} \equiv \bar{s}(1 - \gamma_5)d, \quad (45)$$

which is equal to $\alpha^{(3,\bar{3})}\text{Tr}(\lambda_6\Sigma)$ to lowest order in ChPT, where in our conventions, $\alpha^{(3,\bar{3})} = -\frac{f^2}{2}B_0$.

We briefly review the use of CPS symmetry [23] to determine the form of the power divergences that enter our computations due to mixing with the lower dimensional operator of Eq. 45. Here C and P are the usual charge conjugation and parity inversion symmetries, while S is the symmetry under exchange of the s and d quarks, which is exact when the quark masses are equal.

The parity even part of the above operator, $\bar{s}d$, has a CPS of +1, while the parity odd part, $\bar{s}\gamma_5 d$, has a CPS of -1. The operator, Q_6^{QNS} , has a CPS of +1 and the matrix element $\langle 0|Q_6^{QNS}|K\rangle$ is a parity odd transition. Therefore, the power divergence of this matrix element must be proportional to the matrix element of a lower dimensional operator which is also parity odd and has CPS=+1. We see that the only operator with these symmetries that can be constructed is $\bar{s}\gamma_5 d$ multiplied by $m_s - m_d$. Thus, the power divergent part of $\langle 0|Q_6^{QNS}|K\rangle$ is proportional to $m_s - m_d$.

For the parity even transition, $\langle \pi|Q_6^{QNS}|K\rangle$, the mixing must be with a parity even lower dimensional operator with CPS= +1. In this case the only such operators are $\bar{s}d$ and $(m_s + m_d)\bar{s}d$. The former is ruled out by chiral symmetry. As domain wall fermions at finite L_s break chiral symmetry such a mixing can occur, albeit greatly suppressed due to the domain wall fermion mechanism. Thus, the dominant part of the power divergence of the

$K \rightarrow \pi$ matrix element is proportional to $m_s + m_d$. Since this is a statement at the operator level, it is true to all orders in the chiral expansion, an important result when dealing with the numerical data of a lattice calculation.

We now wish to consider matrix elements of the operator \tilde{Q}_6^{QNS} , since this will give us α_q^{NS} at $O(p^0)$ in the chiral expansion. In order to proceed, we construct a new graded symmetry, $\text{CP}\tilde{\text{S}}$, where now $\tilde{\text{S}}$ not only exchanges s and d quarks, but also exchanges all valence quarks with their corresponding ghosts, *i.e.* under $\tilde{\text{S}}$ the six ‘‘quark’’ fields transform as

$$(u, d, s, \tilde{u}, \tilde{d}, \tilde{s}) \rightarrow (\tilde{u}, \tilde{s}, \tilde{d}, u, s, d). \quad (46)$$

In order to implement this $\text{CP}\tilde{\text{S}}$ symmetry, we need to understand how C and P act on ghost quark states.

Under C , the valence quarks have the following familiar transformation properties

$$q \rightarrow C\bar{q}^T, \quad (47)$$

$$\bar{q} \rightarrow -q^T C^{-1}. \quad (48)$$

Thus, the quark bilinears, $\bar{s}d$ and $\bar{s}\gamma_\mu d$ transform as,

$$\bar{s}d \rightarrow \bar{d}s, \quad (49)$$

$$\bar{s}\gamma_\mu d \rightarrow -\bar{d}\gamma_\mu s, \quad (50)$$

where we have used the identities, $C^\dagger = C^{-1}$ and $C^{-1}\gamma_\mu C = -\gamma_\mu^T$ and the fact that the quark fields anti-commute.

In the case of ghost quarks we can define C analogously to the case of valence quarks, such that

$$\tilde{q} \rightarrow C\tilde{\bar{q}}^T. \quad (51)$$

However, the anti-ghost does not transform independently from the ghost, because it obeys bose statistics. Taking the transpose conjugate of both sides yields

$$\tilde{\bar{q}} \rightarrow \tilde{q}^T C^{-1}, \quad (52)$$

which differs in sign from Eq. 48. Using the transformation rules in Eqs. 51 and 52 and the fact that ghost quark fields commute, we see that

$$\tilde{\bar{s}}\gamma_\mu \tilde{d} \rightarrow -\tilde{d}\gamma_\mu \tilde{s}, \quad (53)$$

where the sign change demonstrates that this transformation for ghost quarks does indeed act as a charge conjugation. For bilinears that are made of a valence quark and an antighost quark the fact that the fields commute will cause a sign change compared to Eqs. 49 and 50. For example,

$$\bar{s}\gamma_\mu\tilde{d} \rightarrow \bar{\tilde{d}}\gamma_\mu s. \quad (54)$$

Under P , the quark fields transform as

$$q \rightarrow Pq, \quad (55)$$

$$\bar{q} \rightarrow \bar{q}P, \quad (56)$$

where $P^\dagger P = 1$. It is simple to recognize that the same transformation under parity is also valid for the ghost fields.

We are now ready to examine the CP \tilde{S} transformation properties of the relevant operators. The bilinear, $\bar{s}\tilde{d}$, has a CP \tilde{S} of -1 , while $\bar{s}\gamma_5\tilde{d}$ has a CP \tilde{S} of $+1$. The four quark operator, \tilde{Q}_6^{QNS} , has a CP \tilde{S} of $+1$. Thus, the matrix element, $\langle 0|\tilde{Q}_6^{QNS}|\tilde{K}\rangle$, which is a parity odd transition, must have a power divergence given by the matrix element of a lower dimensional operator which is both parity odd and has CP $\tilde{S}=+1$. We see that the bilinear operator $\bar{s}\gamma_5\tilde{d}$, which already has the same CP \tilde{S} as \tilde{Q}_6^{QNS} , can only have the coefficient $m_s + m_d$. This is opposite to the situation for the $K \rightarrow 0$ amplitude, where the CPS of Q_6^{QNS} and $\bar{s}\gamma_5 d$ was opposite, implying a power divergence proportional to $m_s - m_d$. The reason for the difference is the exchange of valence and ghost quarks in the right-handed part of Eq. 42 under \tilde{S} , yielding an extra relative minus sign.

Note, this same conclusion could also be reached by starting with the dimension-3 operator which represents the quadratic divergence present in the usual operator Q_6 :

$$\bar{q}\lambda_6 M(1 + \gamma^5)q + \bar{q}M^\dagger\lambda_6(1 - \gamma^5)q = (m_d + m_s)\bar{s}d + (m_d - m_s)\bar{s}\gamma^5 d. \quad (57)$$

Note, the form of the left-hand-side of Eq. 57 is determined by the chiral symmetry properties of the matrix λ_6 (an element of $(8, 1)$) and the quark mass matrix M (an element of $(3, \bar{3})$). The relative sign of the two terms on the left-hand-side of this equation is determined by CPS symmetry. The corresponding dimension-3 operator that mixes with \tilde{Q}_6^{QNS} must have the same form except for the addition of the matrix \bar{A} and a quenched chiral rotation of λ_6 to $\tilde{\lambda}_6$ to agree with the quenched chiral symmetry properties of \tilde{Q}_6^{QNS} :

$$\bar{\mathcal{Q}}\tilde{\lambda}_6 M\bar{A}(1 + \gamma^5)\mathcal{Q} + \bar{\mathcal{Q}}\bar{A}M^\dagger\tilde{\lambda}_6(1 - \gamma^5)\mathcal{Q} = (m_s - m_d)\bar{s}\tilde{d} - (m_s + m_d)\bar{s}\gamma^5\tilde{d}. \quad (58)$$

This argument demonstrates that $\tilde{K} \rightarrow 0$ has a power divergence proportional to $m_s + m_d$. When the fermion discretization does not preserve exact chiral symmetry (such as domain wall fermions with finite L_s), there will also be mixing with the operator $\bar{s}\gamma^5 d$. For domain wall fermions this is suppressed by a power of m_{res} . Such power divergences lead to large uncertainties when one tries to obtain the chiral limit of a matrix element without exact chiral symmetry on the lattice. However, these symmetry arguments suggest a way around this difficulty and we provide an alternative method for obtaining α_q^{NS} in Section VI which makes use of the following observation: the matrix element $\langle \tilde{\pi} | \tilde{Q}_6^{QNS} | K \rangle$ is parity even and since the parity even bilinear, $\bar{s}\tilde{d}$, has $\text{CP}\tilde{S} = -1$, the divergence of $K \rightarrow \tilde{\pi}$ must be proportional to $m_s - m_d$. For degenerate quark masses, the power divergence vanishes completely. Again, this is a statement at the operator level and holds to all orders in the chiral expansion.

C. Lattice contractions for Golterman and Pallante's method

Continuing the derivation of Ref. [12], we carry out the Wick contractions for $\langle 0 | \tilde{Q}_{penguin}^{QNS} | \tilde{K}^0 \rangle$, where we specialize to the case, $Q_{penguin}^{QNS} = Q_6^{QNS}$,

$$\begin{aligned} \langle 0 | \tilde{Q}_6^{QNS} | \tilde{K}^0 \rangle &= -i \sum_{q \in \{u, d, s\}} [I_M(V, A, q) - I_M(A, V, q)] \\ &\quad + \frac{1}{2} [iI'_M(V, A, d) - iI'_M(A, V, d) + iI'_M(V, A, s) - iI'_M(A, V, s)], \end{aligned} \quad (59)$$

with

$$\begin{aligned} I_M(j, k, q) &\equiv \text{Tr}_c \{ \text{Tr}_s [\Gamma_j S_d(x_{op}, x_0) S_s(x_{op}, x_0)^\dagger \gamma_5] \\ &\quad \times \text{Tr}_s [\Gamma_k S_q(x_{op}, x_{op})] \}, \end{aligned} \quad (60)$$

$$\begin{aligned} I'_M(j, k, q') &\equiv \text{Tr}_s \{ \text{Tr}_c [\Gamma_j S_d(x_{op}, x_0) S_s(x_{op}, x_0)^\dagger \gamma_5] \\ &\quad \times \text{Tr}_c [\Gamma_k S_{q'}(x_{op}, x_{op})] \}. \end{aligned} \quad (61)$$

In these contractions, $\Gamma_V = \gamma_\mu$ and $\Gamma_A = \gamma_\mu \gamma_5$ and the traces are over spin or color. The quantity $S_q(x, y)$ is the Dirac propagator connecting positions x and y for a quark of type $q = (u, d, s)$. The position x_0 locates the source for the \tilde{K}^0 meson while x_{op} is the position of the operator \tilde{Q}_6^{QNS} . The derivation of Eq. 59 makes use of the fact that ghost and valence propagators are equal flavor by flavor (when properly ordered; see Appendix B). As discussed

in Ref. [12], this is important because it allows us to obtain α_q^{NS} from contractions that have already been computed for $\langle 0|Q_6^{QCD}|K^0\rangle$.

Golterman and Pallante make the additional observation that the linear combination of contractions for $\langle 0|Q_6^{QNS}|K^0\rangle$ is the same as Eq. 59, but with opposite sign for all but the $I'_M(j, k, d)$ terms. However, a careful treatment of the conventions for external ghost states shows that the $\tilde{K} \rightarrow 0$ matrix element has the opposite sign compared to that given in Golterman and Pallante [14], so that the contractions for $\langle 0|Q_6^{QNS}|K^0\rangle$ are the same as Eq. 59, but with opposite sign for *only* the $I'_M(j, k, d)$ terms. Thus, since $K \rightarrow 0$ does not contribute at $O(p^0)$, subtracting $K \rightarrow 0$ from $\tilde{K} \rightarrow 0$ yields

$$\begin{aligned} \langle 0|\tilde{Q}_6^{QNS}|\tilde{K}^0\rangle - \langle 0|Q_6^{QNS}|K^0\rangle &= i[I'_M(V, A, d) - I'_M(A, V, d)] \\ &= \frac{4i}{f}\alpha_q^{NS} + O(p^2). \end{aligned} \quad (62)$$

Again, we point out that the $O(p^2)$ terms are multiplied by a quadratic divergence in the lattice spacing.

Using the leading order ChPT result,

$$\langle 0|\Theta^{(3,\bar{3})}|K^0\rangle = \frac{2i}{f}\alpha^{(3,\bar{3})} = -\langle 0|\bar{s}\gamma_5 d|K^0\rangle, \quad (63)$$

we obtain the following ratio:

$$\frac{\langle 0|\tilde{Q}_6^{QNS}|\tilde{K}^0\rangle - \langle 0|Q_6^{QNS}|K^0\rangle}{\langle 0|\bar{s}\gamma_5 d|K^0\rangle} = -2\frac{\alpha_q^{NS}}{\alpha^{(3,\bar{3})}} + \frac{\text{const.}}{a^2}m_d + O(p^2). \quad (64)$$

Since we are dividing by precisely the matrix element that, according to the operator level discussion of the previous section, multiplies the power divergence, Eq. 64 explicitly gives the form of the power divergence, with the neglected higher order terms in the chiral expansion being free of these divergences. Again, α_q^{NS} can be obtained in the chiral limit. The power divergence of Eq. 64 is proportional to m_d , since it is the sum of two terms, one proportional to $m_s + m_d$ and the other one proportional to $m_s - m_d$, with the m_s term cancelling between them. The only divergent term in this ratio depends linearly on m_d as shown in Eq. 64. However, after this term proportional to m_d has been removed by extrapolation to $m_d \rightarrow 0$ there remains an $O(m_{res}/a^2)$ contribution for domain wall fermions, due to the power divergence and the lack of exact chiral symmetry for finite L_s [2]. For our simulations, this

effect could be as large as the constant we are trying to extract, as we show in the next subsection.

V. NUMERICAL RESULTS FOR α_q^{NS} FROM $\tilde{K} \rightarrow 0$

We now examine the ratio of matrix elements of Eq. 64, which can be obtained from the contractions given in Eq. 59 and the value for $\langle 0|\bar{s}\gamma_5 d|K\rangle$. We briefly review the details of the ensemble used in Ref. [2] to generate the needed contractions.

The quenched configurations were generated with the Wilson gauge action at a coupling of $\beta = 6.0$ with lattice volume $16^3 \times 32$. The ensemble is comprised of 400 configurations, separated by 10,000 sweeps, with each sweep consisting of a simple two-subgroup heat-bath update of each link (Cabibbo-Marinari with Kennedy-Pendleton accept-reject step). The lattice cut-off was $a^{-1} = 1.922(40)$ GeV set by the ρ mass. The domain wall fermion fifth dimension was $L_s = 16$ sites with a domain wall height $M_5 = 1.8$. The resulting residual quark mass was 0.00124(5) in lattice units. For comparison, the value of m_f corresponding to a pseudo-scalar state made of degenerate quarks with mass equal to the physical kaon at $\beta = 6.0$ is approximately 0.0185. The light quark masses in units of the lattice spacing were taken to be $m_f = 0.01, 0.02, 0.03, 0.04$ and 0.05 .

The data for the ratio in Eq. 64 are given in Table I, and are plotted in Fig. 6 as a function of m_d . We see from Eq. 64 that the intercept of this graph allows one to obtain α_q^{NS} , modulo the effects of the residual chiral symmetry breaking. The two lines in Figure 6 represent linear fits to the data, the top one plotted as a function of m_d , while the bottom is the same data plotted against $m_d + m_{res}$. While in the presence of residual chiral symmetry breaking effects neither of these two methods is known to be correct, comparing these two approaches allows us to estimate the order of magnitude of the $O(m_{res})/a^2$ ambiguity. As can be seen the difference is of the order of 30%, suggesting a potentially large uncontrolled error due to the power divergence.

The result of an uncorrelated fit to the form of $\eta_0 + \eta_1(m_d + m_{res})$ was: $\eta_0 = -5.94(14) \times 10^{-3}$, $\eta_1 = -2.0781(33)$, with a χ^2/dof of 1.67(18). The value of α_q^{NS} obtained from this fit was $-1.20(3) \times 10^{-5}$, where the error is statistical only. If one fits the data in Table I to a linear function of m_d (instead of $m_d + m_{res}$), then the α_q^{NS} obtained is $-1.72(3) \times 10^{-5}$. For comparison, the large N_c approximation, Eq. 41, gives a value of $\alpha_q^{NS} = -1.63(48) \times 10^{-5}$

where, again, the error is statistical only. Here we have used the quenched lattice values for f and B_0 reported in the previous RBC works, [2, 24], obtained on lattices with the same size and coupling as those used here to determine α_q^{NS} . In Ref. [24] it was found that $f = 0.0713(53)$ and $B_0 = 1.59(3)$ in the same lattice units, for an earlier set of 85 configurations. We see that there is rough agreement between the large N_c value and the range of values given directly by the lattice $\tilde{K} \rightarrow 0$ matrix element in the chiral limit. Since an α_q^{NS} of this size would cause significant changes in the $K \rightarrow \pi\pi$ amplitude for Q_6 , as mentioned previously, it is crucial to remove the large systematic error due to the residual power divergence.

VI. LATTICE DETERMINATION OF α_q^{NS} FROM $K \rightarrow \tilde{\pi}$

As we proved in Sec. IV B, the matrix element, $\langle \tilde{\pi} | \tilde{Q}_6^{QNS} | K \rangle$, does not have any power divergences when the quark masses are degenerate. To NLO in ChPT, it is given by

$$\langle \tilde{\pi}^+ | \tilde{Q}_6^{QNS} | K^+ \rangle = -\frac{4}{f^2} \alpha_q^{NS} + O(p^2). \quad (65)$$

Again, we have an amplitude where α_q^{NS} can be obtained in the chiral limit, this time without any power divergent ambiguities. As discussed in the next section on numerical fits, the NLO logarithmic term vanishes for this matrix element in the degenerate mass case (See Appendix C for details of this calculation). The combination of contractions needed for the new amplitude (for degenerate quark masses) is

$$\begin{aligned} \langle \tilde{\pi}^+ | \tilde{Q}_6^{QNS} | K^+ \rangle &= -\frac{1}{2} [L_M^8(V) - L_M^8(A)] \\ &+ \sum_{q \in (u, d, s)} [L_M^I(V, q) - L_M^I(A, q)], \end{aligned} \quad (66)$$

with

$$\begin{aligned} L_M^8(j) &\equiv \text{Tr}_s \{ \text{Tr}_c [\Gamma_j S_d(x_{op}, x_1) S_u(x_{op}, x_1)^\dagger \gamma_5] \\ &\times \text{Tr}_c [\Gamma_j S_u(x_{op}, x_0) S_s(x_{op}, x_0)^\dagger \gamma_5] \}, \end{aligned} \quad (67)$$

$$\begin{aligned} L_M^I(j, q) &\equiv \text{Tr}_c \{ \text{Tr}_s [\Gamma_j S_d(x_{op}, x_1) \gamma_5 S_u(x_1, x_0) S_s(x_{op}, x_0)^\dagger \gamma_5] \\ &\times \text{Tr}_s [\Gamma_j S_q(x_{op}, x_{op})] \}. \end{aligned} \quad (68)$$

Here we use the same notation as in Eqs. 60 and 61 and again exploit the fact that the ghost and valence propagators are equal flavor by flavor when properly ordered [12].

VII. NUMERICAL RESULTS FOR α_q^{NS} FROM $K \rightarrow \tilde{\pi}$

The results for the $\langle \tilde{\pi} | \tilde{Q}_6^{QNS} | K \rangle$ matrix element are given in Table. II and plotted in Fig. 7. The chiral limit was obtained by a simple linear extrapolation of the form $d_0 + d_1(m_f + m_{res})$, with $d_0 = 9.80(76) \times 10^{-3}$, $d_1 = 0.624(17)$ and a $\chi^2/\text{dof} = 0.10(11)$. This yields a value of $\alpha_q^{NS} = -1.24(10) \times 10^{-5}$. In this result we neglect the small error in f^2 . It turns out that the linear fit is exact to NLO in ChPT, as a direct one-loop calculation shows that in this degenerate mass case the logarithmic term vanishes. This calculation is discussed in Appendix C.

A comparison between the two methods for obtaining α_q^{NS} , from $K \rightarrow \tilde{\pi}$ and from $\tilde{K} \rightarrow 0$, is shown in Figure 8, where $f^2/(2\alpha^{(3,\bar{3})})\langle \tilde{\pi}^+ | \tilde{Q}_6^{QNS} | K^+ \rangle$ is plotted over the $\tilde{K} \rightarrow 0$ results. With this normalization the $K \rightarrow \tilde{\pi}$ matrix element given in Eq 65 has the same analytical value for the chiral limit (as determined in ChPT) as the $\tilde{K} \rightarrow 0$ formula given in Eqs 64. The $K \rightarrow \tilde{\pi}$ result does not have a divergent part and the smallness of this amplitude in the numerical data compared to the $\tilde{K} \rightarrow 0$ amplitude reflects this fact. The chiral limit agrees within statistical errors for both methods, which is better than expected, given the systematic errors associated with the $\tilde{K} \rightarrow 0$ amplitude.

The NLO contribution to the matrix element $K \rightarrow \tilde{\pi}$ was computed in order to control the systematic error associated with the extrapolation to the chiral limit. The linear fit is exact to NLO since the log term vanishes, and as Fig. 7 illustrates, this fit is quite good. We therefore conclude that the error in our value of α_q^{NS} in lattice units is dominated by the statistical uncertainty, which is around 10%. As mentioned previously, these results are in rough agreement with the large N_c estimate of Ref. [14], and so, as these authors pointed out, the term proportional to α_q^{NS} will have a large numerical effect on the matrix elements of Q_6 .

VIII. CONCLUSION AND OUTLOOK

The application of the quenched approximation to weak decay matrix elements is made more challenging by the combination of 1) the perturbative calculations (in which QCD vacuum polarization effects are important) needed to connect the high energy scale typical of the W , Z and top masses with the low energy scale of the actual decay and 2) the non-

perturbative QCD calculations (in which the quenched approximation might be employed) needed to evaluate the relevant low energy matrix elements. We have demonstrated in some detail how the quenched approximation can be applied to the latter without altering the calculations which underlie the former. The resulting approach is very close to that employed in the two large-scale quenched calculations reported in Refs. [1, 2].

We then reviewed the quenched chiral perturbation theory results for the strong penguin amplitudes relevant for ϵ'/ϵ as presented by Golterman and Pallante [11, 12]. They have shown that a new LEC, α_q^{NS} , contributes to quenched amplitudes of the strong penguin operators (specifically, to Q_6) and they have proposed a lattice method to obtain this new constant.

In Ref. [14], α_q^{NS} was calculated using the large N_c approximation and the value was found to have a large effect on the $K \rightarrow \pi\pi$ matrix element of Q_6 . Such an effect could significantly alter the value of ϵ'/ϵ reported in Ref. [2]. Therefore, we considered it essential that α_q^{NS} be computed directly on the lattice. The method proposed by [12] to use the matrix element of $\tilde{K} \rightarrow 0$ to obtain α_q^{NS} from the lattice was implemented in this paper, but it was shown that this method suffers from ambiguities due to power divergent contributions when evaluated using the domain wall fermion formalism. We have shown that the amplitude, $K \rightarrow \tilde{\pi}$, provides an alternative method to obtain α_q^{NS} from the lattice but without power divergent contributions. We implemented this method and obtained a value of α_q^{NS} which is indeed large enough to have an important effect on the $K \rightarrow \pi\pi$ matrix element for Q_6 , and, therefore, also on the quenched determination of ϵ'/ϵ .

We conclude that we cannot reliably construct the matrix element $\langle \pi^+\pi^- | Q_6 | K^0 \rangle$ within the quenched approximation using quenched ChPT and our lattice data. This is due to the large value of α_q^{NS} , a low energy constant absent outside of the quenched approximation, which was implicitly assumed to be zero in the previous RBC and CP-PACS work. Such a large quenching artifact does not merely make the extraction of $\langle \pi^+\pi^- | Q_6 | K^0 \rangle$ practically difficult, but implies that the quenched approximation itself fails to accurately describe the full theory. In fact, the motivation for the definition of the quenched approximation outlined in Section II is seen to be invalid, given the large differences in the analytic structure of the full and quenched theories. This clearly reduces the physical relevance of such a calculation.

These arguments and results demonstrate that the errors associated with the quenched approximation in the evaluation of the strong penguin operators are likely to be quite sig-

nificant. Definitive answers will clearly have to await dynamical simulations. The first steps in performing such full QCD simulations have been underway for quite some time with two dynamical flavors [17]; the more realistic 2+1 flavor simulations have begun.

ACKNOWLEDGEMENTS

We thank Maarten Golterman for discussions, our RBC colleagues and especially Thomas Blum and Robert Mawhinney for helpful discussions and suggestions. This research was supported in part by the US DOE under Contract No. DE-AC02-98CH10886 (Laiho, Soni), in part by the DOE under grant # DE-FG02-92ER40699 (Columbia), in part by the RIKEN-BNL Research Center (Blum, Dawson, Noaki), in part by the LDRD grant (Blum, Laiho), and in part by the DOE under grant # DE-AC02-76CH03000 (Laiho).

APPENDIX A

The function, F , appearing in the one-loop contribution to $K \rightarrow \pi\pi$ is given by [12]

$$F(m_1^2, m_2^2, p^2) = \sqrt{\lambda\left(1, \frac{m_1^2}{p^2}, \frac{m_2^2}{p^2}\right)} \ln \frac{p^2 + m_1^2 + m_2^2 + p^2 \sqrt{\lambda(1, m_1^2/p^2, m_2^2/p^2)}}{p^2 + m_1^2 + m_2^2 - p^2 \sqrt{\lambda(1, m_1^2/p^2, m_2^2/p^2)}}, \quad (\text{A1})$$

with

$$\lambda(x, y, z) = (x - y + z)^2 + 4xy.$$

APPENDIX B: NORMALIZATION CONVENTIONS

In this appendix we specify the sign and normalization conventions used in this paper. This includes both the fields and operators used in chiral perturbation theory (where we follow in most cases the conventions used in the earlier work of Golterman and Pallante) and the corresponding quantities defined on the quark level where we follow the conventions used in Ref. [2].

Equations (23) and (24) define the relative signs of the pseudo scalar fields ϕ , the pseudo-fermion fields χ and the ghost fields $\tilde{\phi}$ in the sense that a specific pair of $SU(3|3)_L \times SU(3|3)_R$

matrices, (U_L, U_R) will transform these fields in a determined fashion:

$$\Sigma \rightarrow \Sigma' = U_L \Sigma U_R^\dagger. \quad (\text{B1})$$

Note this relation between the fields ϕ , χ and $\tilde{\phi}$ is still somewhat abstract because the 6×6 matrices U_L and U_R contain both commuting and anti-commuting numbers. However, this description will be sufficient for our purposes because these same matrices transform the quark and pseudo-quark fields q and \tilde{q} :

$$\mathcal{Q} \equiv \begin{pmatrix} q \\ \tilde{q} \end{pmatrix} \rightarrow \begin{pmatrix} q' \\ \tilde{q}' \end{pmatrix} = U_R \begin{pmatrix} q_R \\ \tilde{q}_R \end{pmatrix} + U_L \begin{pmatrix} q_L \\ \tilde{q}_L \end{pmatrix} = (U_R P_R + U_L P_L) \mathcal{Q}. \quad (\text{B2})$$

Here $P_{R/L} = (1 \pm \gamma^5)/2$ and as in the text, \mathcal{Q} contains the three flavors of quarks q and the three flavors of pseudo quarks \tilde{q} and belongs to the Cartesian product representation $SU(3|3)_L \times SU(3|3)_R$.

The absolute normalization and sign for the Σ field is determined by the lowest order effective chiral Lagrangian for quenched QCD:

$$\mathcal{L}_{QCD}^{(2)} = \frac{f^2}{8} \text{str} \{ \partial_\mu \Sigma^\dagger \partial^\mu \Sigma \} + \frac{B_0 f^2}{4} \text{str} \{ M^\dagger \Sigma + \Sigma^\dagger M \} \quad (\text{B3})$$

(written in Minkowski-space) once we specify that the parameter B_0 is real and positive with a magnitude chosen so that the 6×6 matrix M is the quark mass matrix appearing in the fundamental QCD Lagrangian written below.

The Dirac fields q and \tilde{q} are conventional, with the Minkowski space Lagrangian given in terms of \mathcal{Q} by

$$\mathcal{L} = \bar{\mathcal{Q}} i \gamma^\mu D_\mu \mathcal{Q} - \bar{\mathcal{Q}} (M^\dagger P_L + M P_R) \mathcal{Q}. \quad (\text{B4})$$

The connection between quark fields and the corresponding quantities in the effective chiral Lagrangian is given by the equation:

$$(\mathcal{Q}_L)_j (\bar{\mathcal{Q}}_R)_i = \frac{B_0 f^2}{4} \Sigma_{j,i}. \quad (\text{B5})$$

This equation is a generalization of the usual relation between Σ and the quark fields to include the new variables which appear in the quenched case. It is uniquely determined by the combined requirements of flavor covariance (the left and right-hand sides transform identically under the $SU(3|3)_L \times SU(3|3)_R$ flavor transformations of Eqs. (B1) and (B2)) and consistency with the equation for the chiral condensate:

$$\langle \bar{u}_R u_L \rangle = \frac{i \partial}{\partial M_{11}^\dagger} \ln Z[M, M^\dagger] = -\frac{B_0 f^2}{4} \langle \Sigma_{11} \rangle, \quad (\text{B6})$$

where we examine the condensate associated with the up quark, the first component of \mathcal{Q} , and treat the matrix elements $M_{1,1}$ and $M_{1,1}^*$ as independent variables. Note, the flavor covariance of Eq. (B5) is lost and the resulting equation invalid if the order of the factors $(\mathcal{Q}_R)_j$ and $(\overline{\mathcal{Q}}_L)_i$ is reversed, since these 6-component fields are a mixture of commuting and anti-commuting quantities.

Following standard conventions, we identify the field ϕ in Eq. (24) with meson fields according to:

$$\phi = \begin{pmatrix} \pi^0/\sqrt{2} + \eta/\sqrt{6} & \pi^+ & K^+ \\ \pi^- & -\pi^0/\sqrt{2} + \eta/\sqrt{6} & K^0 \\ K^- & \overline{K}^0 & -2\eta/\sqrt{6} \end{pmatrix}, \quad (\text{B7})$$

where the specific fields appearing in Eq. (B7) above destroy the corresponding mesons. Similarly the ghost field χ of Eq. 24 can be written in an identical fashion if a tilde is added to each of the meson fields, *e.g.* π^+ is replaced by $\tilde{\pi}^+$. With these conventions we can then examine specific components of Eq. (B5) to lowest order in chiral perturbation theory and obtain the useful relations:

$$\overline{s}\gamma^5 d = iB_0 f K^0 \quad (j=2, i=3), \quad (\text{B8})$$

$$\overline{s}\gamma^5 \tilde{d} = -iB_0 f \tilde{K}^0 \quad (j=5, i=3). \quad (\text{B9})$$

This same identification can be made by an appropriate generalization of the results in Appendix A of Ref. [2] to the quenched case.

Remaining consistent with Eq. (B5), we can easily write down expressions relating quark-level operator states and chiral-level operator states. For a given meson operator in terms of the underlying quark fields, we have

$$\overline{d}\gamma_5 s|0\rangle = iB_0 f \overline{K}^0|0\rangle = iB_0 f|K^0\rangle, \quad (\text{B10})$$

$$\tilde{d}\gamma_5 s|0\rangle = -iB_0 f (\tilde{K}^0)^\dagger|0\rangle = -iB_0 f|\tilde{K}^0\rangle, \quad (\text{B11})$$

where Eq. (B10) is the standard relation between states in terms of the quark-level and chiral operators. Eq. (B11) is found by a chiral rotation on Eq. (B10) to give the corresponding relation between these fermionic meson states. To be concrete, we also include here the rules needed for evaluating matrix elements of operators with these χ fields. These are given by chiral rotations on the appropriate K^0 field rules, and found to be

$$\langle 0|\tilde{K}^0(x)|\tilde{K}^0(k)\rangle = e^{ikx}, \quad (\text{B12})$$

and

$$\langle \tilde{K}^0(\mathbf{k}') | \tilde{K}^0(\mathbf{k}) \rangle = 2E_K (2\pi)^3 \delta^3(\mathbf{k}' - \mathbf{k}) . \quad (\text{B13})$$

Unlike the standard meson fields like K^0 , the ordering in these expressions is rather important, since $\tilde{K}^0(\tilde{K}^0)^\dagger = -(\tilde{K}^0)^\dagger \tilde{K}^0$. Additionally, as stated earlier in the text, the quark and ghost-quark propagators are equal flavor by flavor (when properly ordered), such that

$$\langle 0 | d(x) \bar{d}(y) | 0 \rangle = \langle 0 | \tilde{d}(x) \tilde{\bar{d}}(y) | 0 \rangle = S_F(x, y) , \quad (\text{B14})$$

where $(\gamma_\mu D_\mu + m)S_F(x, y) = \delta^{(4)}(x - y)$, for the case of continuum, Euclidean fermions.

Next we apply this same approach to relate the various components of the four-quark operator related to Q_6^{QNS} as they appear in chiral perturbation theory and at the quark level:

$$\mathcal{O}_{ji}^{QNS} \equiv \text{tr}_D \{ (Q_L)_j^a (\gamma^\mu)^t (\bar{Q}_L)_i^b \} \text{tr}_D \{ \text{str} [Q_R^b (\gamma^\mu)^t \bar{Q}_R^a \bar{A}] \} = \alpha_q^{NS} \left(\Sigma \bar{A} \Sigma^\dagger \right)_{j,i} \quad (\text{B15})$$

where the diagonal matrix \bar{A} is defined in Eq. (21), a and b are color indices, tr_D is a trace over the (implied) Dirac indices, and we are exploiting flavor covariance and the conventions of Ref. [15]. We can use this expression to evaluate two cases of importance by using $(\lambda_6)_{ij} = \delta_{i3}\delta_{j2}$ and $(\tilde{\lambda}_6)_{ij} = \delta_{i3}\delta_{j5}$. In other words, multiplying Eq. (B15) by either λ_6 or $\tilde{\lambda}_6$ and taking the supertrace over the $SU(3|3)$ indices, we get

$$Q_6^{QNS} = \text{str} [\lambda_6 \mathcal{O}^{QNS}] + \text{h.c.} = \alpha_q^{NS} \text{str} (\lambda_6 \Sigma \bar{A} \Sigma^\dagger) + \text{h.c.} , \quad (\text{B16})$$

$$\tilde{Q}_6^{QNS} = \text{str} [\tilde{\lambda}_6 \mathcal{O}^{QNS}] + \text{h.c.} = \alpha_q^{NS} \text{str} (\tilde{\lambda}_6 \Sigma \bar{A} \Sigma^\dagger) + \text{h.c.} , \quad (\text{B17})$$

which are precisely the expressions we see in Eqs. (14) and (19) for Q_6^{QNS} , and Eqs. (42) and (43) for \tilde{Q}_6^{QNS} .

APPENDIX C

The NLO corrections to $K \rightarrow \tilde{\pi}$ are calculated from one-loop insertions of the operator Eq. 43, as well as local operators that begin at NLO:

$$\tilde{\mathcal{O}}_1^{NS} = \text{tr}[\tilde{\lambda}_6 L_\mu \Sigma^\dagger \bar{A} \Sigma L^\mu], \quad (\text{C1})$$

$$\tilde{\mathcal{O}}_2^{NS} = \text{tr}[\tilde{\lambda}_6 L_\mu] \text{tr}[\Sigma^\dagger \bar{A} \Sigma L^\mu], \quad (\text{C2})$$

$$\tilde{\mathcal{O}}_3^{NS} = \text{tr}[\tilde{\lambda}_6 \{\Sigma^\dagger \bar{A} \Sigma, L^2\}], \quad (\text{C3})$$

$$\tilde{\mathcal{O}}_4^{NS} = \text{tr}[\tilde{\lambda}_6 \{\Sigma^\dagger \bar{A} \Sigma, S\}], \quad (\text{C4})$$

$$\tilde{\mathcal{O}}_5^{NS} = \text{tr}[\tilde{\lambda}_6 [\Sigma^\dagger \bar{A} \Sigma, P]], \quad (\text{C5})$$

$$\tilde{\mathcal{O}}_6^{NS} = \text{tr}[\tilde{\lambda}_6 \Sigma^\dagger \bar{A} \Sigma] \text{tr}[S]. \quad (\text{C6})$$

Each operator has associated with it an a priori unknown LEC which we call \tilde{c}_i^{NS} , with a scale dependence similar to that of Eq 32,

$$\tilde{c}_i^{r,NS}(\mu_2) = \tilde{c}_i^{r,NS}(\mu_1) + \frac{2\alpha_q^{NS} \tilde{\eta}_i}{(4\pi f)^2} \ln \frac{\mu_1}{\mu_2}. \quad (\text{C7})$$

The coefficient of the scale dependence, $\tilde{\eta}_i$, can be determined as in [25], where the authors apply background field and heat bath methods. The values for $\tilde{\eta}_i$ are 0, -2 , $-N_f/2$, $N_f/2$, 0 and 1 for $i = 1 - 6$ respectively. In this case N_f is the number of sea quarks, which for the quenched case should naively be taken to zero. However one must take care in this case because this operator (Eq 43) has been introduced precisely to add contractions of the four quark operators that contribute to the fermion determinant which would otherwise be absent in the quenched approximation in which we are working.

We can determine the scale dependence in the quenched theory by making use of the following trick. In the partially quenched case, $\bar{A} \rightarrow \bar{A}_{PQ} = 2(1 - 3/N_f, 1 - 3/N_f, 1 - 3/N_f, -3/N_f, \dots, -3/N_f)_{\text{diag}}$, where the first 3 valence entries are $1 - 3/N_f$, and the next $N_f + 3$ ghost and sea entries are $-3/N_f$. Taking the $N_f \rightarrow 0$ limit in this matrix is singular, but when these factors multiply the $\tilde{\eta}_i$ factors above, this limit yields the correct scale dependence for the amplitudes in the quenched theory.

The scale dependence obtained in this way agrees with that of a direct one-loop calculation of $K \rightarrow \tilde{\pi}$, which yields precisely zero in the case of degenerate quarks. Thus, the one-loop chiral log vanishes, and the only NLO contribution in the degenerate case is proportional to m_M^2 ($m_f + m_{res}$ in fits to DW fermions) with an unknown coefficient. The diagrams needed are given in Fig. 9. The wave-function renormalization vanishes for $\tilde{\pi}$ and K for this matrix

element.

-
- [1] J. I. Noaki *et al.* (CP-PACS), Phys. Rev. **D68**, 014501 (2003), hep-lat/0108013.
 - [2] T. Blum *et al.* (RBC), Phys. Rev. **D68**, 114506 (2003), hep-lat/0110075.
 - [3] V. Fanti *et al.* (NA48), Phys. Lett. **B465**, 335 (1999), hep-ex/9909022.
 - [4] J. R. Batley *et al.* (NA48), Phys. Lett. **B544**, 97 (2002), hep-ex/0208009.
 - [5] A. Alavi-Harati *et al.* (KTeV), Phys. Rev. Lett. **83**, 22 (1999), hep-ex/9905060.
 - [6] A. Alavi-Harati *et al.* (KTeV), Phys. Rev. **D67**, 012005 (2003), hep-ex/0208007.
 - [7] S. Eidelman *et al.* (Particle Data Group), Phys. Lett. **B592**, 1 (2004).
 - [8] D. Pekurovsky and G. Kilcup, Phys. Rev. **D64**, 074502 (2001), hep-lat/9812019.
 - [9] T. Bhattacharya *et al.*, Nucl. Phys. Proc. Suppl. **140**, 369 (2005), hep-lat/0409046.
 - [10] C. Bernard, T. Draper, A. Soni, H. D. Politzer, and M. B. Wise, Phys. Rev. **D32**, 2343 (1985).
 - [11] M. Golterman and E. Pallante, JHEP **10**, 037 (2001), hep-lat/0108010.
 - [12] M. Golterman and E. Pallante, Phys. Rev. **D69**, 074503 (2004), hep-lat/0212008.
 - [13] M. Golterman and E. Pallante (2006), hep-lat/0602025.
 - [14] M. Golterman and S. Peris, Nucl. Phys. Proc. Suppl. **129**, 311 (2004), hep-lat/0309101.
 - [15] M. Golterman and S. Peris, Phys. Rev. **D68**, 094506 (2003), hep-lat/0306028.
 - [16] C. W. Bernard and M. F. L. Golterman, Phys. Rev. **D46**, 853 (1992), hep-lat/9204007.
 - [17] Y. Aoki *et al.* (2004), hep-lat/0411006.
 - [18] M. A. Clark, A. D. Kennedy, and Z. Sroczynski (2004), hep-lat/0409133.
 - [19] P. H. Damgaard and K. Splittorff, Phys. Rev. **D62**, 054509 (2000), hep-lat/0003017.
 - [20] B. S. DeWitt Cambridge, UK: Univ. Pr. (1992) 407 p. (Cambridge monographs on mathematical physics). (2nd ed.),.
 - [21] M. Golterman and E. Pallante, JHEP **08**, 023 (2000), hep-lat/0006029.
 - [22] J. Laiho and A. Soni (2003), hep-lat/0306035.
 - [23] C. W. Bernard, T. Draper, G. Hockney, and A. Soni, Nucl. Phys. Proc. Suppl. **4**, 483 (1988).
 - [24] T. Blum *et al.*, Phys. Rev. **D69**, 074502 (2004), hep-lat/0007038.
 - [25] V. Cirigliano and E. Golowich, Phys. Lett. **B475**, 351 (2000), hep-ph/9912513.

TABLE I: The ratio $(\langle 0|\tilde{Q}_6^{QNS}|\tilde{K}\rangle - \langle 0|Q_6^{QNS}|K\rangle)/\langle 0|\bar{s}\gamma_5 d|K\rangle$ for each of ten nondegenerate pairs of quark masses. The chiral limit of this ratio ($m_d \rightarrow 0$) can be used to obtain α_q^{NS} .

m_s	$m_d = 0.01$	$m_d = 0.02$	$m_d = 0.03$	$m_d = 0.04$
0.02	$-2.898(13) \times 10^{-2}$			
0.03	$-2.918(13) \times 10^{-2}$	$-5.010(13) \times 10^{-2}$		
0.04	$-2.932(13) \times 10^{-2}$	$-5.020(12) \times 10^{-2}$	$-7.088(13) \times 10^{-2}$	
0.05	$-2.941(13) \times 10^{-2}$	$-5.026(12) \times 10^{-2}$	$-7.093(13) \times 10^{-2}$	$-9.141(14) \times 10^{-2}$

TABLE II: The matrix element $\langle \tilde{\pi}|\tilde{Q}_6^{QNS}|K\rangle$ as a function of m_f , the single quark mass that appears in the degenerate kaon and pion states. The chiral limit of this data can be used to obtain α_q^{NS} using Eq. 65.

m_f	$\langle \tilde{\pi} \tilde{Q}_6^{QNS} K\rangle$
0.01	$1.702(69) \times 10^{-2}$
0.02	$2.293(68) \times 10^{-2}$
0.03	$2.910(70) \times 10^{-2}$
0.04	$3.545(72) \times 10^{-2}$
0.05	$4.199(74) \times 10^{-2}$

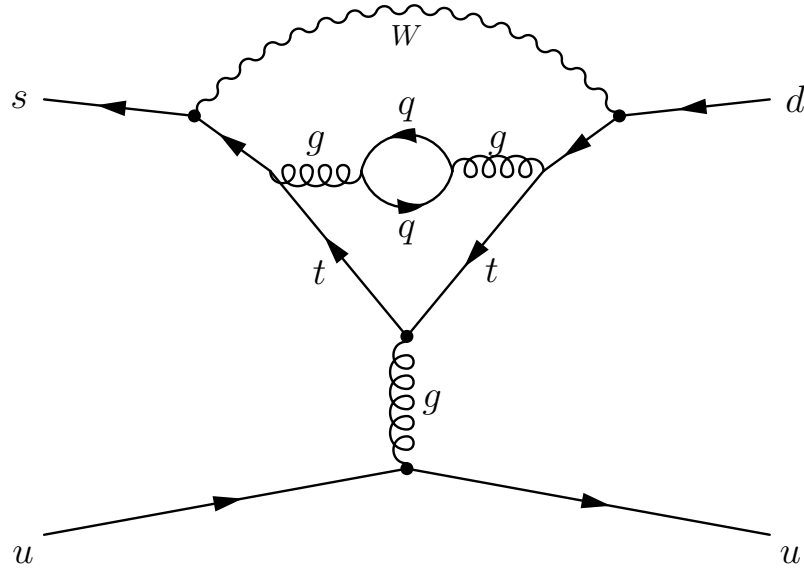


FIG. 1: A $K^+ \rightarrow \pi^+$ diagram in which the vacuum polarization loop is entirely contained within a high-momentum subgraph.

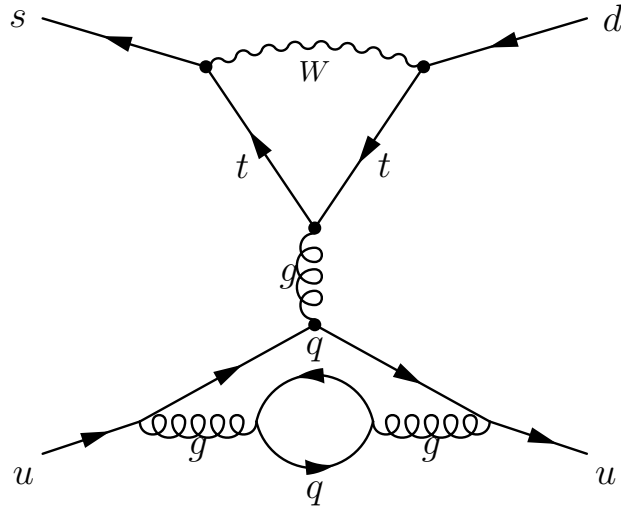


FIG. 2: A $K^+ \rightarrow \pi^+$ diagram in which the vacuum polarization subgraph must appear entirely within a low-momentum subgraph.

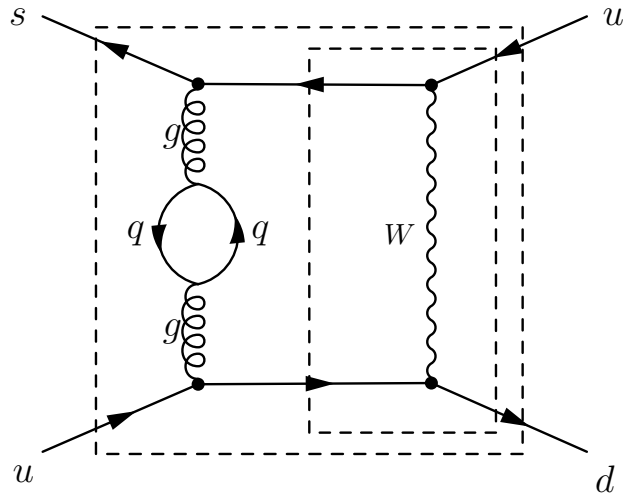


FIG. 3: A $K^+ \rightarrow \pi^+$ diagram in which the vacuum polarization subgraph must be wholly inside or outside of any high-momentum subgraph.

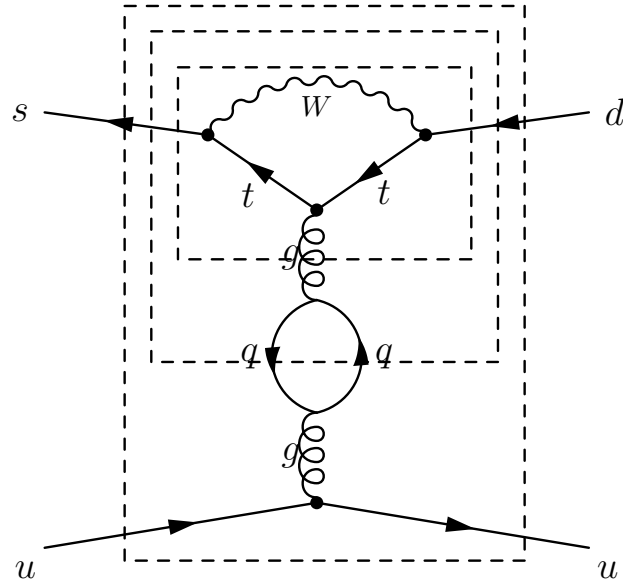


FIG. 4: A $K^+ \rightarrow \pi^+$ diagram in which the vacuum polarization subgraph can be partially contained within a high-momentum subgraph.

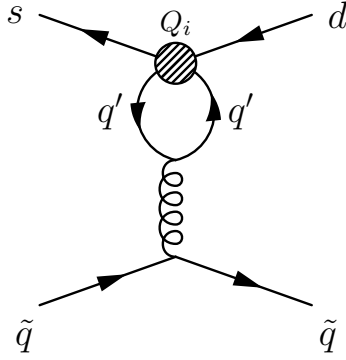


FIG. 5: An order α_s diagram which generates a non-vanishing ghost amplitude in a quenched theory from operators with no direct ghost quark coupling.

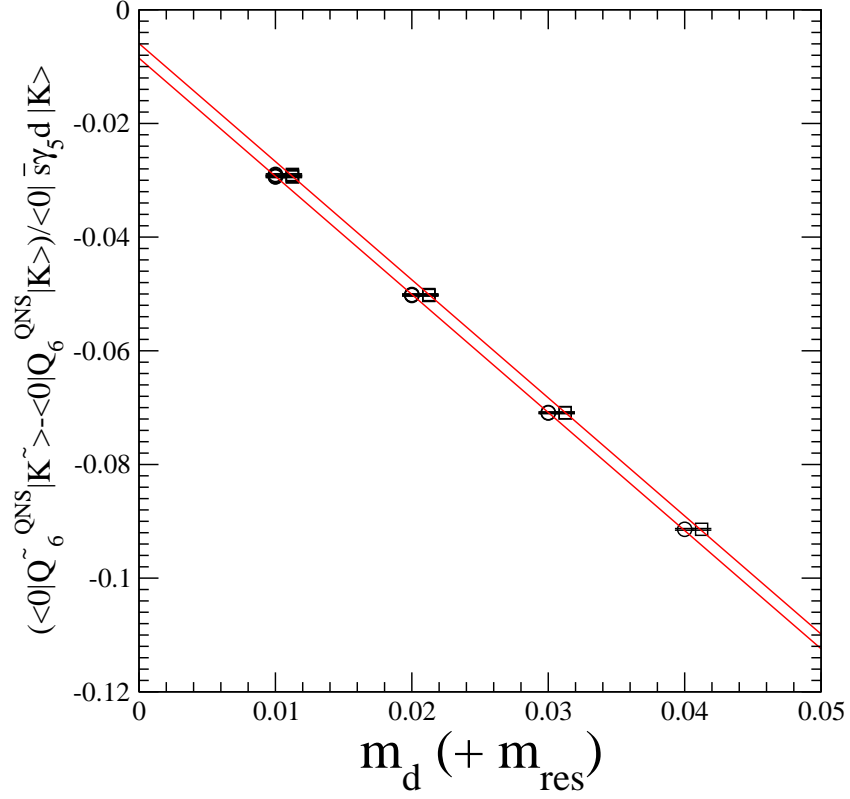


FIG. 6: The ratio $(\langle 0 | \tilde{Q}_6^{QNS} | \tilde{K} \rangle - \langle 0 | Q_6^{QNS} | K \rangle) / \langle 0 | \bar{s} \gamma_5 d | K \rangle$ versus m_d (circles) and $m_d + m_{res}$ (squares) for the ten nondegenerate quark masses. The lines are linear fits to the data of the form $\eta_0 + \eta_1 m_d$ and $\eta_0 + \eta_1 (m_d + m_{res})$.

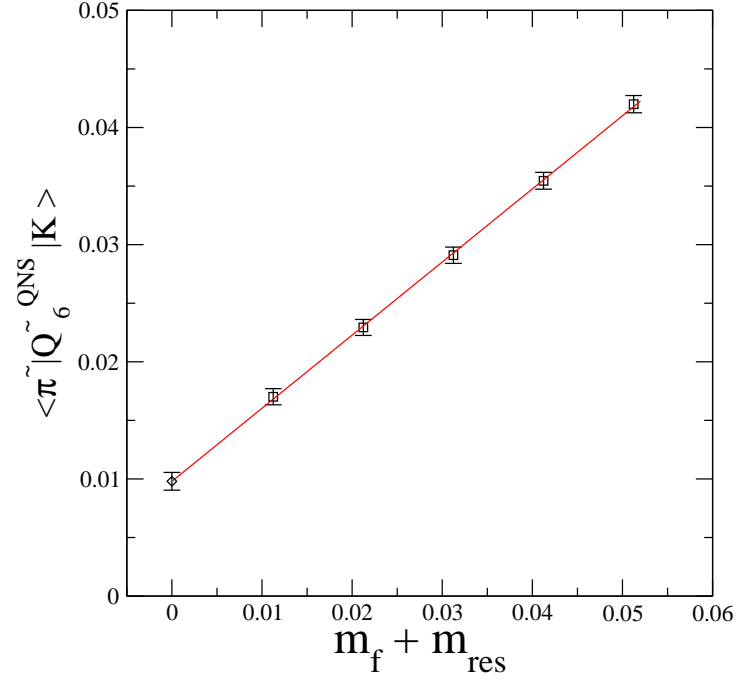


FIG. 7: The matrix element $\langle \tilde{\pi} | \tilde{Q}_6^{QNS} | K \rangle$ as a function of $m_f + m_{res}$. The solid line is a simple linear fit to the data and the intercept can be used to obtain α_q^{NS} from Eq. 65.

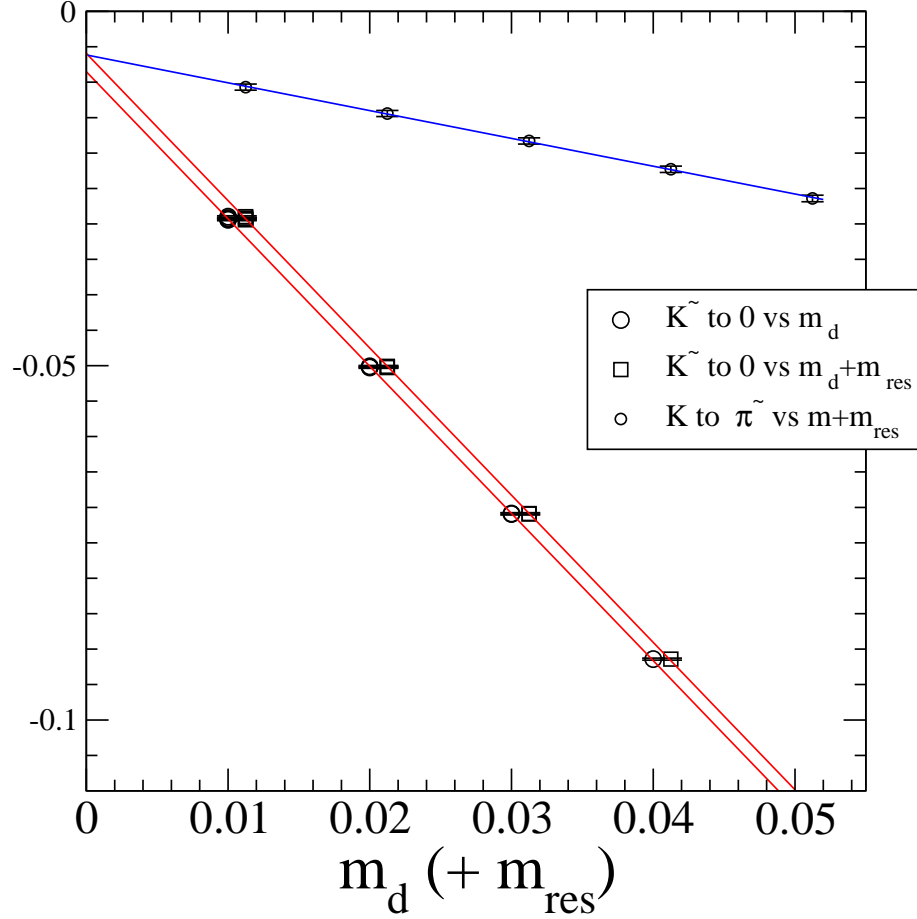


FIG. 8: The matrix elements $(\langle 0 | \tilde{Q}_6^{QNS} | \tilde{K} \rangle - \langle 0 | Q_6^{QNS} | K \rangle) / \langle 0 | \bar{s} \gamma_5 d | K \rangle$ as a function of m_d (big circles) and $m_d + m_{res}$ (squares) and $f^2 / (2\alpha^{(3, \bar{3})}) \langle \tilde{\pi} | \tilde{Q}_6^{QNS} | K \rangle$ (small circles) as a function of m_d equal to the degenerate masses of the quarks appearing in the K meson. For comparison, we plot the $\tilde{K} \rightarrow 0$ matrix elements above. The pre-factor of $\langle \tilde{\pi} | \tilde{Q}_6^{QNS} | K \rangle$ re-scales the matrix element so that the chiral limits of the two methods are expected to agree according to ChPT. This graph shows that the chiral limits do agree, thus yielding similar values of α_q^{NS} .

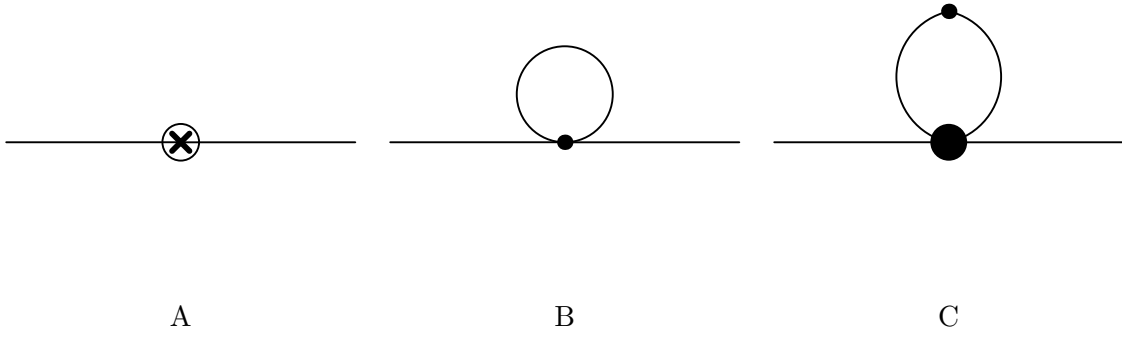


FIG. 9: Diagrams needed to evaluate the NLO amplitude $K \rightarrow \tilde{\pi}$. NLO corrections include tree-level diagrams with insertion of the NLO weak vertices (crossed circle), one-loop diagrams with insertions of the LO weak vertices (small filled circles) and the $O(p^2)$ strong vertices (big filled circle). The lines represent the propagators of mesons comprised of valence and ghost quarks.